Journal of Materials Chemistry A

REVIEW

View Article Online
View Journal | View Issue

Cite this: J. Mater. Chem. A, 2020, 8, 16081

Controlled colloidal metal nanoparticles and nanoclusters: recent applications as cocatalysts for improving photocatalytic water-splitting activity

Tokuhisa Kawawaki,[ab] Yutaro Mori,[a] Kosuke Wakamatsu,[a] Shuhei Ozaki,[a] Masanobu Kawachi,[a] Sakiat Hossain[a] and Yuichi Negishi*[ab]

In recent years, research on the use of metal nanoparticles (NPs) and nanoclusters (NCs) synthesized by liquid-phase reduction in water-splitting photocatalysts has been actively conducted. Water-splitting photocatalysts have been attracting attention because they can produce hydrogen (H_2), which is attractive as a next-generation energy source, from solar energy and water. However, further improvement of water-splitting photocatalysts is required for their practical use in society. Recent studies have demonstrated that the active sites (cocatalysts) of water-splitting photocatalysts can be controlled using the advanced NP/NC syntheses and structural modulation techniques established in the fields of colloid, NP, and NC chemistry and thereby highly active water-splitting photocatalysts can be developed. If such research progresses further, it is expected that a transition to a new society using H_2 as the main energy source will become possible. However, such applied research has just started and examples of such research are currently limited. The purpose of this review is to introduce the importance of controlled colloidal NPs/NCs in research on water-splitting photocatalysis to readers by summarizing the existing research. We hope that this review will raise interest in the application of metal NPs/NCs in water-splitting photocatalysis and that a society actively addressing energy and environmental problems will become a reality as soon as possible.

Received 7th May 2020
Accepted 22nd July 2020

DOI: 10.1039/d0ta04750c

rsc.li/materials-a

[a]Department of Applied Chemistry, Faculty of Science, Tokyo University of Science, 1-3 Kagurazaka, Shinjuku-ku, Tokyo 162-8601, Japan. E-mail: negishi@rs.tus.ac.jp; Fax: +81-3-5261-4631; Tel: +81-3-5228-9145

[b]Research Institute for Science & Technology, Tokyo University of Science, 1-3 Kagurazaka, Shinjuku-ku, Tokyo 162-8601, Japan

1. Introduction

1.1. Metal nanoparticles and nanoclusters

The nanometer scale is the smallest on which the function of a material appears. Therefore, if a material can be controlled at

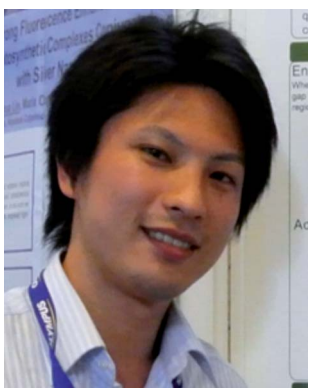

Tokuhisa Kawawaki. Assistant professor of the department of applied chemistry at Tokyo University of Science. He received PhD degree (2015) in applied chemistry from the University of Tokyo. Since 2016, he worked as Japan Society for the Promotion of Science (JSPS) Postdoctoral fellow (PD) at the University of Melbourne. Since 2017, he worked as JSPS super PD (SPD) at Kyoto University. In 2019, he moved to the current position. His current research topics include synthesis of metal nanoparticles and nanoclusters in solution and their applications for photoelectrochemistry and photocatalysts.

Yutaro Mori. Master course student in the Negishi group at Tokyo University of Science. He received his BSc (2018) and MSc (2020) in chemistry from Tokyo University of Science. His research interests include the activation of water-splitting photocatalysts by controlling cocatalysts.

the nanometer scale, almost all the properties of the material can be regulated. Furthermore, it is possible to produce new physical/chemical properties and functions different from those of the bulk material by controlling the atomic array structure (crystal structure) at the nanometer scale. Because of the importance of and interest in producing nanomaterials with intended structure and function, technology to control nanomaterials (*i.e.*, nanotechnology) is being promoted as a national policy in many countries.

Metal nanoparticles (NPs) (Fig. 1),[1,2] which are aggregates of metal atoms, play a central role in such nanotechnology research. Research on metal NPs was initiated by Faraday in the 1840s in his investigation of metal colloids.[3] Since the 1980s, the research on metal colloids has progressed substantially and the expression "metal NPs" has been coined.[4–23] In the last two decades, research on metal NPs has increased explosively, and the techniques to synthesize metal NPs have advanced dramatically. In recent years, it has become possible to control not only the size of metal NPs but also their geometrical structure. Metal NPs composed of coinage metals such as gold (Au), silver (Ag), and copper (Cu) exhibit localized surface plasmon resonance absorption in the visible region (Fig. 1),[23–27]

Kosuke Wakamatsu. Master course student in the Negishi group at Tokyo University of Science. He received his BSc (2018) and MSc (2020) in chemistry from Tokyo University of Science. His research interests include the elucidation of key parameter for improving water-splitting photocatalysts.

Shuhei Ozaki. Master course student in the Negishi group at Tokyo University of Science. He received his BSc (2019) in chemistry from Tokyo University of Science. In 2019, he worked as a study abroad student at The University of Adelade (Greg Metha's group). His research interests include the activation of visible-light driven water-splitting photocatalysts.

Masanobu Kawachi. Master course student in the Negishi group at Tokyo University of Science. He received his BSc (2020) in chemistry from Tokyo University of Science. His research interests include the activation of visible-light driven water-splitting photocatalysts.

Sakiat Hossain. Postdoctoral researcher in the Negishi group at Tokyo University of Science. He obtained his BSc (2005) from Ramakrishna Mission Residential College, Narendrapur, Calcutta University, MSc (2007) from the Indian Institute of Technology Delhi, and PhD (2013) from the Indian Institute of Technology Kanpur under the supervision of Prof. V. Chandrasekhar. He joined Tokyo University of Science in 2015. His research interests include the synthesis of novel metal clusters and study of their properties.

Yuichi Negishi. Professor of the department of applied chemistry at Tokyo University of Science. He received his PhD degree in chemistry in 2001 under the supervision of Prof. Atsushi Nakajima from Keio University. Before joining Tokyo University of Science in 2008, he was employed as an assistant professor at Keio University and at the Institute for Molecular Science. His current research interests include the precise synthesis of stable and functionalized metal nanoclusters and their applications in energy and environmental materials.

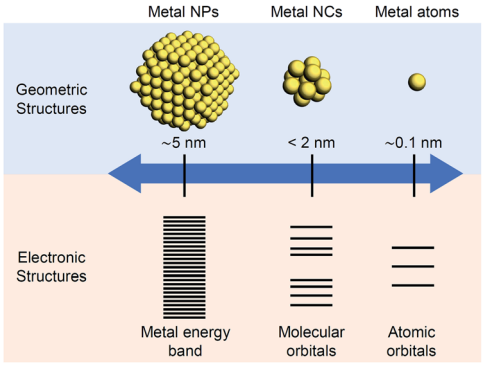

Fig. 1 Comparison of metal NPs, NCs, and atoms.

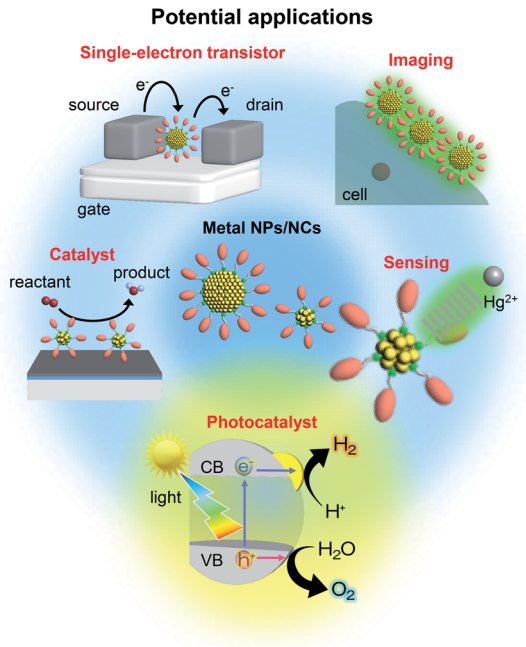

Fig. 2 Potential applications of metal NPs and NCs.

which makes these NPs even more attractive. Because of these properties, metal NPs can be used in surface-enhanced Raman spectroscopy.[28] Therefore, studies on the use of metal NPs to detect trace amounts of molecules are being conducted for applications.[29] In addition, techniques to control the arrangement of metal NPs have been established,[30] which has opened the way to apply metal NPs in the field of electronic devices. Furthermore, metal NPs are also expected to be useful in biotechnology applications such as drug delivery systems and diagnosis (Fig. 2).[31]

Metal nanoclusters (NCs), as shown in Fig. 1, are smaller in size than metal NPs and are also important materials in nanotechnology.[32,33] There is no clear definition of the boundary between metal NPs and metal NCs. However, when the particle size is less than 2 nm, the materials are generally called metal NCs (Fig. 1). Such ultrafine metal NCs possess electronic and geometrical structures that are different from those of both the corresponding bulk metal and metal NPs, which leads to the appearance of new physical/chemical properties and functions (Fig. 1).[34–45] Furthermore, because the physical/chemical properties and functions of NCs strongly depend on the number of constituent atoms, if the number of constituent atoms in metal NCs can be controlled, numerous functions can be realized by one metal element. When multiple elements are used in NCs, it is possible to access further various functions.[46–56]

Gas-phase experiments played a leading role in research on metal NCs in the 1980s and 90s.[57–69] Also, the synthesis of metal NCs composed of gold, palladium (Pd), and platinum (Pt) started at that time.[70–78] However, it was only after 2000 that research on these NCs began to increase explosively.[79] In 2005, the first precise synthesis method for thiolate (SR)-protected metal NCs was established.[80] Since then, numerous noble metal and alloy NCs have been precisely synthesized using SR, phosphine, and alkyne ligands.[81–109] Since 2007, it has become possible to determine the geometrical structure of NCs by single-crystal X-ray diffraction (XRD) analysis.[110–114] Thus, at present, inorganic chemists precisely synthesize SR-protected metal NCs as organic chemists synthesize organic molecules. It is possible to obtain a deep understanding of the structure–property relationship of metal NCs with precisely determined geometrical structure.[82–114] The use of these well-defined NCs as catalysts, chemical sensors, photosensitizers, and solar cell components is currently being studied (Fig. 2).[34,79,115–122]

In this way, the syntheses and applications are being actively investigated for metal NPs and metal NCs at present. Multiple reviews have been published on the recent research development of such metal NPs and NCs.[34,79,115–122] Readers hoping to obtain comprehensive knowledge of the synthesis techniques of metal NPs/NCs, their geometrical structures, and potential applications should refer to these reviews.

1.2. Application of metal NPs/NCs as cocatalysts in water-splitting photocatalysts

This review outlines the research on the use of metal NPs/NCs in the field of water-splitting photocatalysis, in which many groups have begun to work in recent years (Fig. 2). With the

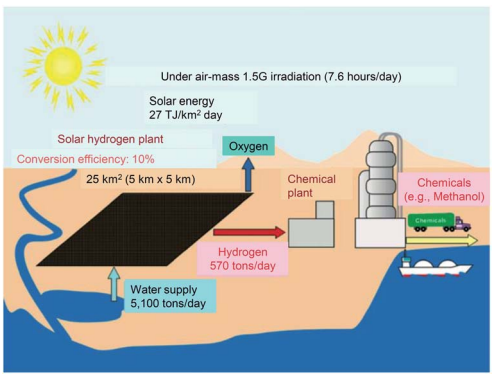

Fig. 3 Possible scheme for large-scale H_2 production *via* solar water splitting. Reproduced with permission from ref. 124. Copyright 2010 American Chemical Society.

depletion of fossil resources and the aggravation of climate change, the transition from a society that depends on fossil fuels to one that uses clean and renewable energy is needed. Hydrogen (H_2) releases a large amount of energy upon combustion. In addition, the combustion of H_2 generates only water, which does not pollute the environment. Thus, H_2 has great potential as a new energy source that solves energy and environmental problems (Fig. 3).

Most H_2 is currently produced by steam reforming of fossil resources. However, this method releases carbon dioxide as a byproduct and consumes fossil resources. Therefore, if H_2 continues to be produced by this method, it will not provide a solution for both energy and environmental problems. The water-splitting photocatalytic reaction[123] has been proposed as a clean and renewable H_2 production method (Fig. 3).[124] Using this reaction, it is possible to produce H_2 from sunlight and water, which are available in almost unlimited quantities on the earth. This is different from the case of the water-splitting electrocatalytic reaction[125–128] in which electric power is consumed to proceed the reaction (thus, the combination with the solar cells is indispensable in this case[129,130]). However, although water-splitting photocatalysts have been attracting attention for many years, further improvement is still required to realize their practical use.

Water-splitting semiconductor photocatalysts are often composed of semiconductor photocatalysts and metal NP/NC cocatalysts that work as reaction sites (Fig. 4).[131] The cocatalyst plays a role in promoting the photocatalytic reaction, and it has been shown that control of the cocatalyst particle size and dispersion improves photocatalytic activity. However, it is difficult to control the particle size and chemical composition of cocatalysts loaded using conventional photodeposition and impregnation methods because the metal NPs/NCs are grown on the surface of the photocatalyst in these methods (Fig. 5A).[132,133] To overcome these problems and produce highly active water-splitting photocatalysts suitable for practical use, it is essential to introduce new techniques for the preparation of water-splitting photocatalysts.

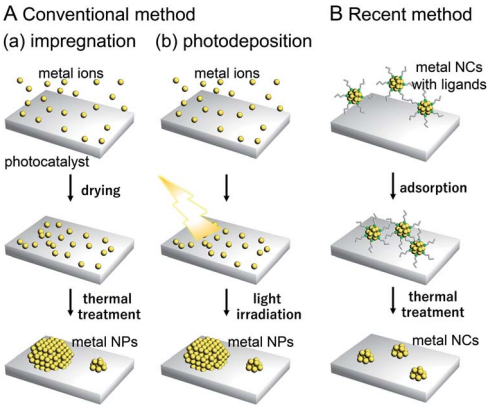

Fig. 5 Comparison of (A) conventional and (B) recent cocatalyst loading methods. As conventional methods, (a) impregnation and (b) photodeposition methods are shown in (A).

As described in Section 1.1, techniques to control the particle size distribution of metal NPs fabricated by liquid-phase synthesis have already been established. When such controlled metal NPs are adsorbed on a photocatalyst and the surface protective organic molecules (ligand, polymer, *etc.*) are removed, it is possible to obtain controlled metal NP-loaded photocatalysts with high water-splitting activity (Fig. 5B).[132,133] When precisely controlled metal NCs are used as the precursor, it is possible to regulate the

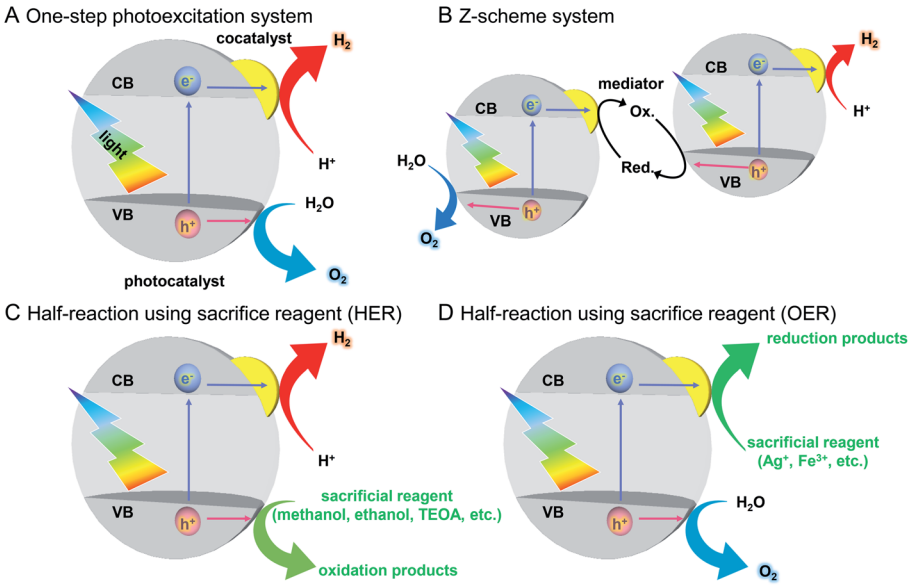

Fig. 4 Schematics of photocatalytic reactions. (A) One-step photoexcitation system for overall water splitting, (B) Z-scheme system for overall water splitting, and half reactions using a sacrificial reagent; (C) H_2 evolution reaction (HER) and (D) O_2 evolution reaction (OER). VB and CB mean the valence and conduction band, respectively.

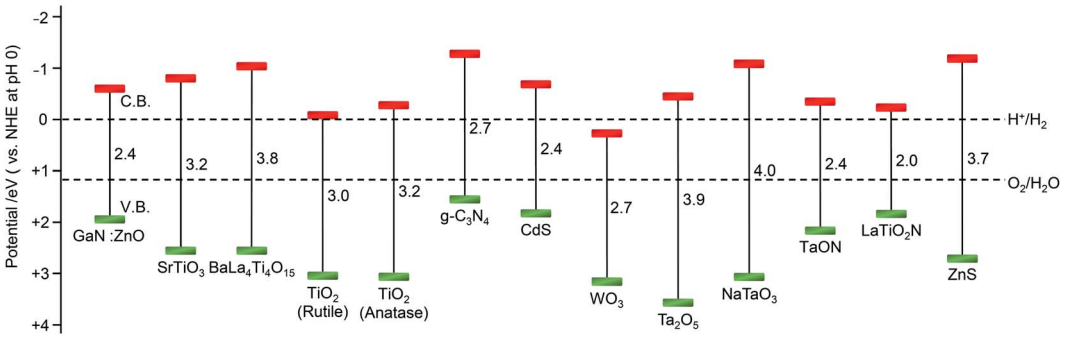

Fig. 6 Relationship between the semiconductor band structure and redox potentials of water splitting. Reproduced with permission from ref. 145–147, and 160. Copyright 2009 Royal Society of Chemistry, Copyright 2020 Royal Society of Chemistry, Copyright 2018 Royal Society of Chemistry, and Copyright 2010 American Chemical Society.

cocatalyst on a photocatalyst with atomic precision.[134–136] For such precise metal NCs, detailed information about electronic and geometrical structures can be obtained by various high-resolution measurements and theoretical calculations, as shown in the previous studies on the supported metal NPs/NCs.[118,137] Therefore, loading the cocatalyst controlled with atomic accuracy would lead to the clear design guidelines for high activation of water-splitting photocatalysts. If appropriate metal NCs are designed and fabricated based on the knowledge obtained in this way, the activity of water-splitting photocatalysts is expected to be further enhanced.

1.3. Purpose of this review

As described in Section 1.2, water-splitting photocatalysts can be activated using cocatalysts fabricated by precise synthesis and structure control techniques (nanotechnology) established in the fields of colloid, NP, and NC chemistry. Such highly active water-splitting photocatalysts could lead to the resolution of energy and environmental problems. However, such applied research has only recently started, and at present the examples are limited. The purpose of this review is to introduce the importance of using controlled colloidal metal NPs/NCs in research on water-splitting photocatalysis by summarizing the existing research. We hope that this review will increase interest in the application of metal NPs/NCs in water-splitting photocatalysts. Ultimately, it is anticipated that the progress of this research will lead to a society in which energy and environmental problems have been solved.

1.4. Contents of this review

This review is constituted as follows. First, Section 2 provides an overview of water-splitting photocatalysts. Then, Section 3 outlines the methods used to load cocatalysts. Section 4 presents examples of research using metal NPs/NCs fabricated by liquid-phase synthesis as cocatalysts in water-splitting photocatalysts. In this section, we also present examples of studies using metal NPs/NCs for H_2 or O_2 production from water (the half reactions of water splitting), although these reactions do not realize complete decomposition of water. Section 5 shows the importance of elucidating the interface between metal NPs/NCs and substrates, and introduces appropriate methods for such a purpose. Section 6 summarizes this review, and Section 7 briefly describes the prospects of metal NPs/NCs in water splitting.

It should be noted that there are many studies using NPs/NCs not as active sites but as light absorption sites in water-splitting photocatalysis.[138–144] A number of reviews on the use of NPs/NCs as photosensitizers have already been published,[37,115] so this review does not cover such research.

2. Water-splitting photocatalysts

2.1. Reaction mechanism

As described in Section 1.2, a water-splitting photocatalyst generally consists of a semiconductor photocatalyst and cocatalyst. When the photocatalyst is irradiated with light, electrons are excited from the valence band (VB) to the conduction band (CB) in the semiconductor photocatalyst. The excited electrons in the CB and holes remaining in the VB move to the photocatalyst surface and/or cocatalyst, where the electrons reduce water and the holes oxidize water (Fig. 4).[131,132] Theoretically, if the bottom edge of the CB of the semiconductor photocatalyst is more negative than the reduction potential of water (0 V *vs.* normal hydrogen electrode; NHE), the reduction reaction of water proceeds and H_2 is produced; this is called the H_2 evolution reaction (HER). In addition, if the top edge of the VB of the semiconductor photocatalyst is more positive than the oxidation potential of water (1.23 V *vs.* NHE), the oxidation reaction of water proceeds and O_2 is produced, which is called the O_2 evolution reaction (OER) (Fig. 6).[145–147] However, a semiconductor that satisfies these conditions is not always capable of completely decomposing water (*i.e.*, overall water splitting), which is largely related to the following factors: (i) the high activation energy of water splitting makes it difficult for this reaction to proceed; (ii) the reaction is deactivated by recombination of electrons and holes; and (iii) the produced H_2 and O_2 can undergo the reverse reaction. Therefore, it is important to suppress these negative factors when designing a cocatalyst.

2.2. Reaction system

The recent major systems used for the water-splitting reaction are one-step photoexcitation systems[148] and two-step photoexcitation systems (*i.e.*, Z-scheme systems).[131,132,147,149–152] In

addition to these systems, much research has been conducted on the half reactions of water splitting (HER, OER) using sacrificial agents. Here, these reactions are outlined.

2.2.1. One-step photoexcitation systems. In one-step photoexcitation systems, water is completely decomposed by a single semiconductor photocatalyst (Fig. 4A). These one-step photoexcitation systems for water-splitting photocatalysis originated from the Honda–Fujishima effect[123] reported in 1972. Early research mainly focused on the development of photocatalysts only photoexcited by ultraviolet (UV) light.[153–155] These studies produced many UV-active water-splitting photocatalysts with high quantum yields.

On the other hand, to realize the practical application of water-splitting photocatalysis, it is necessary to use visible light, which accounts for about 40% of solar energy. As described in Section 2.1, to completely decompose water, the positions of the CB and VB of a photocatalyst must be at appropriate energies to enable the HER and OER, respectively. Furthermore, to suppress recombination of excited electrons and holes, the photocatalyst needs to have high crystallinity and large specific surface area. Because of these requirements, only a limited number of photocatalysts for one-step photoexcitation systems that can completely decompose water with visible light have been reported.[151]

2.2.2. Z-scheme systems. There are few semiconductor photocatalysts that satisfy the following three factors: (i) absorption of visible light; (ii) suitable energy levels for overall water splitting; and (iii) appropriate properties including high stability and non-toxicity. However, if a semiconductor that can catalyze the HER is combined with another that catalyzes the OER and a redox couple that transfers charges (electrons and holes) between them, overall water splitting is possible. Such a system, which imitates photosynthesis in plants, is called a Z-scheme system (Fig. 4B).[132,147]

Z-scheme systems include semiconductor photocatalysts that proceed a half reaction of water splitting (HER or OER). Therefore, compared with the case for one-step photoexcitation systems, there are many photocatalysts available, and it is possible to use a longer wavelength of sunlight. Additionally, because the HER and OER occur on different photocatalysts, it is possible to suppress the reverse reaction between the generated H_2 and O_2 by using a two-cell reaction tube with an ion-exchange membrane. Also, an operation to separate the generated gas is unnecessary. However, in Z-scheme systems, the reverse reaction involving a redox couple occurs, which is different from the case for one-step photoexcitation systems. Furthermore, because two photons are required for one reaction in overall water splitting, Z-scheme systems have the disadvantage of lower theoretical conversion efficiency than that of one-step photoexcitation systems.

2.2.3. Half reactions using sacrificial reagents. As described above, overall water splitting by a semiconductor photocatalyst is generally difficult to achieve. Therefore, the photocatalytic ability of a semiconductor to drive each half-reaction (HER, OER) is often evaluated using an electron/hole trapping agent, which is called a sacrificial agent. For example, when light is irradiated on water containing a hole trapping agent (methanol, ethanol, ascorbic acid, or triethanolamine (TEOA)) that is more easily oxidized than water, the holes generated by photoexcitation are preferentially used to oxidize the hole trapping agent. Therefore, the reduction of protons (H^+) by photoexcited electrons is likely to occur and H_2 is easily produced. These measurements can evaluate the HER ability of a cocatalyst without being affected by OER activity (Fig. 4C). Similarly, when the activity of the water-splitting reaction is measured in water containing an electron trapping agent (such as Ag^+ or Fe^{3+}), water oxidation is likely to occur, so the OER activity of various photocatalysts can be easily evaluated (Fig. 4D). Measurement of the activity of such a half reaction is very important for determining whether a photocatalyst satisfies some of the requirements for water splitting and for exploring photocatalysts that could be used in Z-scheme systems.

2.3. Semiconductor photocatalyst materials

Semiconductors used as photocatalysts are mainly metal oxides, metal nitrides, and metal sulfides (Fig. 6).[131,151] Also, metal-free graphitic carbon nitride (g-C_3N_4) can be used as a water-splitting photocatalyst.[148,156,157] Metal oxides generally have high stability but do not readily absorb visible light because their VB mainly consists of oxygen 2p orbitals and is located to the positive side of the redox potential of the OER. To overcome these problems, the following strategies have been used to modify photocatalysts: (i) metal-ion doping ($SrTiO_3$: Rh, Ir[158,159]); (ii) formation of solid solutions (GaN:ZnO,[160] ZnS–$AgInS_2$–$CuInS_2$,[161] $La_5Ti_2Cu_{0.9}Ag_{0.1}S_5O_7$,[162] $In_{0.2}Ga_{0.8}N$,[163] *etc.*); (iii) controlling the VB position by including elements other than oxygen ($BiVO_4$,[164–166] TaON,[167,168] Ta_3N_5,[168] *etc.*); and (iv) using a dye sensitization reagent (Ru(II) complex[169]).

2.4. Cocatalyst materials

The cocatalyst promotes the transfer of electrons and holes generated by photoexcitation and also plays a role in lowering the activation energies of the HER and OER (Fig. 4). Each reaction on the cocatalyst involves the adsorption of the substrate, reaction of the substrate, and desorption of the products. The progress of each reaction is strongly related to the adsorption/desorption energies of the substrate/product on the cocatalyst surface. In particular, the chemical reaction on the cocatalyst surface proceeds easily when the Gibbs energy of formation is moderate for the state where the substrates and products are adsorbed on the cocatalyst. This is because the reaction does not occur without the substrate being adsorbed, but the reaction is inhibited when the adsorption is too strong. Generally, metal or metal oxide NPs composed of group 8–11 elements are used as the cocatalyst because of their suitable binding affinity with substrates. These NPs often have diameters of several to several tens of nanometers.[133,170] Additionally, it has recently been reported that MoS_2 and WS_2 [171] are highly active HER cocatalysts.[170] An important point is that metal/metal oxides NPs/NCs that are highly active in the HER and/or OER but also highly active towards the reverse reactions

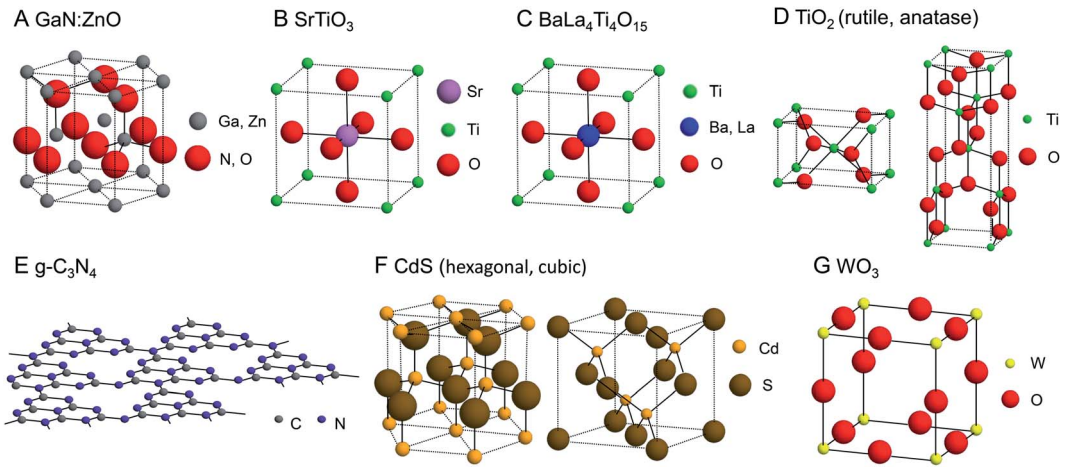

Fig. 7 Geometrical structures of photocatalysts introduced in this review. (A) GaN:ZnO, (B) $SrTiO_3$, (C) $BaLa_4Ti_4O_{15}$, (D) TiO_2, (E) g-C_3N_4, (F) CdS, and (G) WO_3.

cannot be used as cocatalysts. Metal/metal oxides NPs/NCs are generally active in reverse reactions, so when they are used as cocatalysts, formation of core/shell structure, alloy state, or a solid solution is necessary to suppress the reverse reactions on the cocatalyst surface.[147]

2.5. Towards practical use

For the practical use of a water-splitting photocatalyst, the conversion efficiency of solar energy to H_2 (STH) needs to be at least 10%. However, the current maximum STH for water splitting using semiconductor fine particles is about 1.1%.[151,172] Therefore, further improvement of STH is required for the practical use of water-splitting photocatalysts. Among such efforts, the development of visible light-responsive photocatalysts and highly functional cocatalysts are particularly important research subjects. To develop more advanced cocatalysts, it is necessary for the density of active sites to be increased, and the substrate adsorption energy to be optimized by the modulation of the cocatalyst electronic structure. Refinement of the cocatalyst is an effective strategy to achieve both of these characteristics and alloying is also effective for the latter. In addition, techniques for loading fine cocatalyst particles on photocatalysts with high dispersity and improving cocatalyst durability are also important for practical application of water-splitting photocatalysts.

3. Cocatalyst loading methods

3.1. Conventional methods

In previous studies, cocatalysts have been loaded on photocatalysts by impregnation and photodeposition methods. These loading methods are widely used because of their simplicity.

The impregnation method (Fig. 5A(a)) was first used for loading the cocatalysts on the photocatalysts by Domen *et al.* in 1980.[172] Since then, this method has been used as an effective method for loading the cocatalysts. In this method, the photocatalyst and precursor metal salt of the cocatalyst are thoroughly mixed using a mortar and pestle and then calcined to deposit fine cocatalyst particles on the photocatalyst surface. In the photodeposition method (Fig. 5A(b)), a photocatalyst is dispersed in a solution containing a precursor metal salt of the cocatalyst and then light is irradiated on the photocatalyst. The cocatalyst is deposited on the photocatalyst surface through the reduction or oxidation of the metal salt by the electrons or holes generated *via* photoexcitation.[173] Using the photodeposition method, it is possible to preferentially load the cocatalyst particles on a specific crystal plane of the photocatalyst, which become the reaction sites on the photocatalyst surface.[174]

In the catalyst systems fabricated using these two methods, the metal NP/NCs necessarily have a size distribution because the metal atoms are aggregated on the photocatalyst (Fig. 5A).[175] Also, it is not possible to apply methods such as size separation and size convergence to these loaded metal NPs/NCs, unlike metal NPs/NCs dispersed in a solution. Therefore, it is difficult to load cocatalysts with a uniform size on photocatalysts using these conventional methods.

3.2. Recent method using colloidal metal NPs/NCs: liquid-phase adsorption

In recent years, it became possible to synthesize various types of metal NPs/NCs with controlled size and chemical composition in the liquid phase. Colloidal metal NPs/NCs of the same size can be adsorbed on a photocatalyst and then the protective organic molecules are removed, leading to the production of controlled metal NP/NC-loaded photocatalysts. This approach is often called liquid-phase adsorption.

In the liquid-phase adsorption method, first, metal NPs/NCs are adsorbed on the photocatalyst by mixing the metal NPs/NCs and photocatalyst in a solvent. Because metal oxide photocatalysts generally have numerous surface hydroxyl groups (–OH) in water, metal NPs/NCs with protective organic molecules with dissociative functional groups (such as $-CO_2H$, $-SO_3H$, or $-NH_3$ groups) can be adsorbed on the photocatalyst

Table 1 Materials and experimental conditions in the study using liquid-phase adsorption method for overall water-splitting

	Cocatalyst					
Semiconductor	Kinds	Loading amount	Size	Light source	Reactant solution	Ref.
GaN:ZnO	Cr_2O_3/Rh NPs	0.3–0.4 wt%	1.9 ± 0.6 nm	450 W Hg lamp ($NaNO_2$ aq. filter)	Distilled water, 400 mL	176
GaN:ZnO	Cr_2O_3/Rh NPs (adsorption)	2.5 wt%	1.9 ± 0.6 nm	450 W Hg lamp $NaNO_2$ aq. filter)	Distilled water, 370–400 mL	181
	Cr_2O_3/Rh NPs (photodeposition)	1.0 wt%	>2–3 nm			
	Cr_2O_3/Rh NPs (impregnation)	0.25 wt%	>2–3 nm			
GaN:ZnO	Rh NPs	0.1–0.3 wt%	1.5 ± 0.3 nm	450 W Hg lamp ($NaNO_2$ aq. filter)	H_2SO_4 aq. (pH 4.5), 400 mL	182
		0.1–0.3 wt%	3.8 ± 0.8 nm			
		0.1–0.3 wt%	6.6 ± 1.1 nm			
GaN:ZnO	Cr_2O_3/Rh NPs (shell/core), Mn_3O_4 NPs	Rh: 0.75 wt%, Cr: 0.31 wt%, Mn: 0.05 wt%	Cr_2O_3/Rh: >2–3 nm, Mn_3O_4: 9.2 ± 0.4 nm	300 W Xe lamp (λ > 420 nm)	Pure water, 100 mL	184
GaN:ZnO	Cr_2O_3/Rh NPs, Mn_3O_4 NPs	Rh: 0.75 wt%, Cr: 0.31 wt%, Mn_3O_4: 0.2 wt%		300 W Xe lamp (λ > 420 nm)	H_2O, 100 mL	185
	Cr_2O_3/Rh NPs, IrO_2 NPs	Rh: 0.75 wt%, Cr: 0.31 wt%, IrO_2: 0.3 wt%				
	Cr_2O_3/Rh NPs, RuO_2 NPs	Rh: 0.75 wt%, Cr: 0.31 wt%, RuO_2: 0.2 wt%				
$SrTiO_3$	Cr_2O_3/Rh NPs, $Co_xMn_{3-x}O_4$ NPs, (Co/(Co + Mn) ratio of 40 mol%)	Sum of Co and Mn: 0.05 wt%, Rh: 0.3 wt%	$Co_xMn_{3-x}O_4$: 9.0 ± 0.8 nm	300 W Xe lamp (λ > 300 nm)	H_2O, 100 mL	186
		Mn: 0.05 wt%, Rh: 0.3 wt%	9.0 ± 0.5 nm			
$BaLa_4Ti_4O_{15}$	Au_{25}	0.1 wt%	1.2 ± 0.3 nm	400 W Hg lamp	Distilled water, 350 mL	187
	Au NPs	0.5 wt%	10–30 nm			
$SrTiO_3$	Au_{25}	0.1 wt%	~1.2 nm	400 W Hg lamp	Distilled water, 350 mL	188
	Au NPs	0.5 wt%	9.5 ± 3.3 nm			
$BaLa_4Ti_4O_{15}$	Au_{10}	0.1 wt%	0.89 ± 0.19 nm	400 W Hg lamp	Distilled water, 350 mL	189
	Au_{15}	0.1 wt%	0.95 ± 0.21 nm			
	Au_{18}	0.1 wt%	1.12 ± 0.22 nm			
	Au_{25}	0.1 wt%	1.19 ± 0.28 nm			
	Au_{39}	0.1 wt%	1.53 ± 0.26 nm			
$BaLa_4Ti_4O_{15}$	Au_{25}	0.1 wt%	1.1 ± 0.2 nm	400 W Hg lamp	Distilled water, 350 mL	190
	Cr_2O_3/Au_{25}	Cr: 0.5 wt%, Au: 0.1 wt%	1.1 ± 0.3 nm			
$BaLa_4Ti_4O_{15}$	Au_{25}	0.1 wt%	1.24 ± 0.21 nm	400 W Hg lamp	Distilled water, 350 mL	202
	$Au_{24}Pd$	0.1 wt%	1.11 ± 0.19 nm			
	$Au_{24}Pt$	0.1 wt%	1.11 ± 0.19 nm			
$BaLa_4Ti_4O_{15}$	$Rh_{2-x}Cr_xO_3$ NCs	Rh: 0.09 wt%, Cr: 0.10 wt%	1.3 ± 0.3 nm	400 W Hg lamp	Distilled water, 350 mL	208
	$Rh_{2-x}Cr_xO_3$ NCs (impregnation)	Rh: 0.10 wt%, Cr: 0.15 wt%	3.0 ± 2.3 nm			
TiO_2	PtO NCs	0.5 wt%	1.0 ± 0.3	300 W Xe lamp (λ > 300 nm)	Methanol aq.	211
	Pt NCs	1.0 wt%	2.0 ± 0.5 nm			

surface at a high adsorption rate *via* hydrogen bond formation between the protective organic molecules and photocatalyst surface.[176] Even when the protective organic molecules do not have dissociative functional groups, if they contain phenyl groups, the metal NPs/NCs can be adsorbed on the photocatalyst at a relatively high adsorption rate *via* dipole–dipole interactions.[177] After adsorption, the protective organic molecules are removed from the metal NPs/NCs by calcination, photocatalytic oxidation/reduction by light irradiation, or ozone oxidation. This approach has attracted much attention in recent years as a novel method to load photocatalysts with cocatalysts with controlled particle size and chemical composition (Fig. 5B).

4. Application of colloidal metal NPs/NCs

4.1. Application in overall water splitting

This section introduces research using metal NPs/NCs in the overall water-splitting reaction. The photocatalysts used in these studies are summarized in Fig. 7. The materials and conditions used in these studies are summarized in Table 1.

4.1.1. Use of colloidal metal NPs. Domen *et al.*[176] started to use metal NPs synthesized by the liquid-phase reduction method for overall water splitting in 2009. They used monodispersed colloidal rhodium (Rh) NPs as a precursor. The size-controlled Rh NPs (1.9 ± 0.6 nm) were loaded on a GaN:ZnO solid solution,[160] which is a visible light-responsive photocatalyst (Fig. 8 and Table 1). The Rh NPs with a size of 1.7 ± 0.3 nm were synthesized using sodium 3-mercapto-1-propanesulfonate as a ligand (Fig. 8A(a)). This ligand is suitable for the synthesis of small NPs and is easily removed from the NPs by calcination after adsorption on a photocatalyst. Because the sulfonate groups in the ligands of the Rh NPs were not adsorbed at a high rate on the photocatalyst surface, they changed the functional group of the ligands from sulfonate groups to sulfonic acid by cation exchange after NP synthesis (Fig. 8A(b)). This conversion promoted the formation of hydrogen bonds and acid–base interactions between the Rh NPs and photocatalyst surface. Thereby, the Rh NPs were adsorbed on the photocatalyst at a high rate (Fig. 8A(c)). Then, the ligands were removed from the Rh NPs by calcination at 673 K for 30 min under reduced pressure, leaving the Rh NPs loaded on the photocatalyst (Fig. 8A(d)). The particle size of the loaded Rh NPs (1.9 ± 0.6 nm) was about one quarter of that of Rh NPs loaded by the conventional photodeposition method. This indicates that the loading method used in this study is suitable for loading fine NPs on the photocatalyst surface. The researchers formed a Cr_2O_3 shell on the surface of the Rh NPs to suppress the light-induced O_2 reduction reaction (ORR), which is a reverse reaction of water splitting that occurred on the surface of the loaded Rh NPs without a Cr_2O_3 shell. The Cr_2O_3 shell was permeable to H^+ but not O_2 approaching from the outside.[178–180] When the cocatalyst surface was protected by a Cr_2O_3 shell with such characteristics, it was possible to suppress the progress of the reverse reaction while maintaining the H_2 production ability of the catalyst, thereby leading to high water-splitting activity. The team formed Cr_2O_3 shells on the Rh NPs loaded on photocatalysts prepared by both methods (Fig. 8B). The photocatalyst with Rh NPs loaded by the liquid-phase adsorption method exhibited water-splitting activity that was about three times higher than that of the photocatalyst with Rh NPs (7.6 nm) loaded by conventional photodeposition (Fig. 8C). This indicates that miniaturization of the metal core

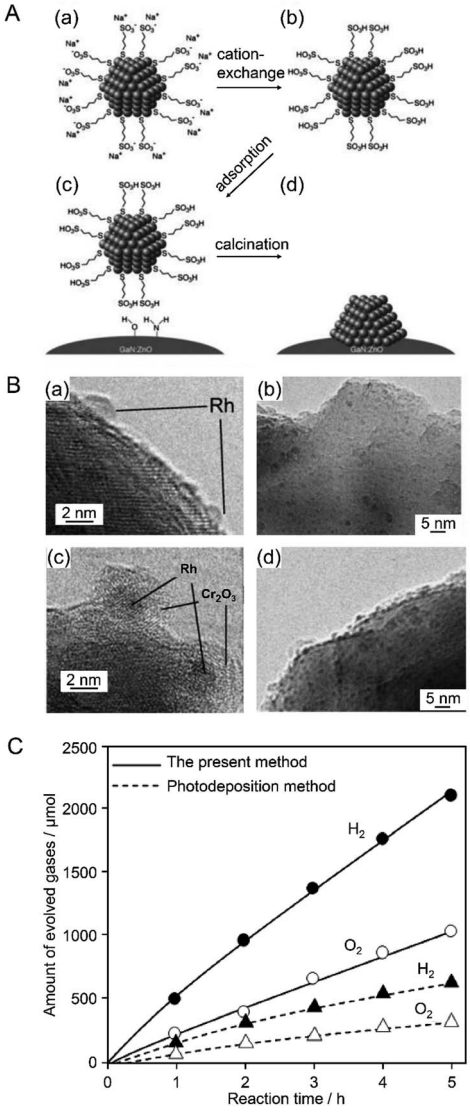

Fig. 8 (A) Procedural flow of the proposed liquid-phase adsorption method: (a) Rh NPs stabilized by organic ligand molecules before cation exchange. (b) Stabilized Rh NPs after cation exchange. (c) Electrostatic adsorption on GaN:ZnO catalyst. (d) Removal of organic ligand. (B) TEM images of Rh NPs loaded on GaN:ZnO (a and b) before and (c and d) after coating with Cr_2O_3. (C) Time course of overall water splitting over Cr_2O_3/Rh/GaN:ZnO prepared by liquid-phase adsorption and photodeposition. Reaction conditions: catalyst, 0.15 g; distilled water, 400 mL; light source, high-pressure mercury lamp (450 W) *via* aqueous $NaNO_2$ solution filter to cut UV light; reaction vessel, Pyrex inner-irradiation vessel. Almost the same amount of Rh (0.3–0.4 wt%) was loaded on each catalyst. Reproduced with permission from ref. 176. Copyright 2009 The Royal Society of Chemistry.

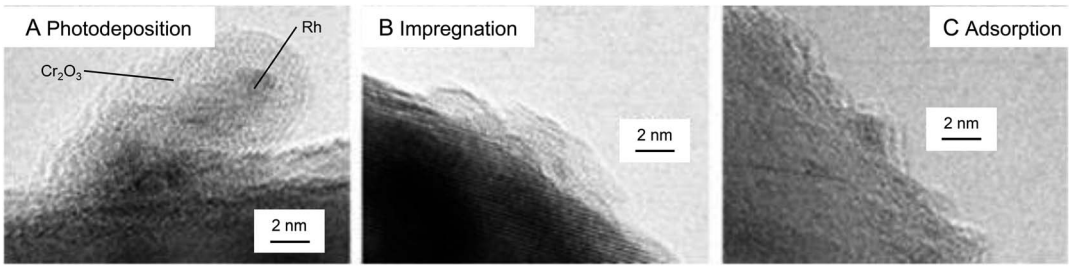

Fig. 9 TEM images of Cr_2O_3/Rh NPs (shell/core)/GaN:ZnO. The core Rh NPs were loaded by (A) photodeposition, (B) impregnation, and (C) liquid-phase adsorption. Reproduced with permission from ref. 181. Copyright 2010 Wiley-VCH.

of the cocatalyst is an effective approach to improve water-splitting activity. The group also reported in this paper that cocatalyst loading by liquid-phase adsorption is also effective for loading NPs composed of other noble metals. When the cocatalyst NPs were composed of Pd or Pt, decreased particle size also enhanced the activity of the NP-loaded GaN:ZnO solid-solution photocatalyst.

In 2010, the same group further developed such research. In this study, various noble metals (Rh, Pd, and Pt) and metal oxides (NiO_x, RuO_2, and Rh_2O_3) were used as HER cocatalysts for GaN:ZnO photocatalysts.[181] Both conventional methods (photodeposition and impregnation methods; Fig. 5A) and liquid-phase adsorption (Fig. 5B) were used to load NPs on the photocatalyst. A Cr_2O_3 shell was also formed on the cocatalyst surface. The highest activity was obtained when Rh was used as the core metal and the cocatalysts were loaded by liquid-phase adsorption. In the liquid-phase adsorption method, Rh cocatalysts with fine particle size can be loaded with high dispersion. Additionally, it is presumed that Rh cocatalysts loaded by liquid-phase adsorption have more metallic properties than those loaded by conventional methods. The photocatalyst with Rh NPs loaded by liquid-phase adsorption was considered to show high water-splitting activity because of these factors. This study also revealed that the morphology of the Cr_2O_3 shell depended on the valence state of the core Rh NPs and pH of the solution during the photodeposition of the Cr_2O_3 layer. Based on this knowledge, they formed a Cr_2O_3 shell with appropriate thickness on metallic Rh NPs at an appropriate pH (3.0–7.5) (Fig. 9), which yielded an efficient water-splitting photocatalyst.

In 2013, to further functionalize the Rh NP cocatalyst, Teranishi and colleagues investigated the correlation between the particle size of Rh NPs and water-splitting activity.[182] In this study, Rh NPs were synthesized by polyol reduction using polyvinylpyrrolidone (PVP, M_w: 10 000 or 40 000) as a protective polymer. The effects of the pH and temperature of the reaction solution (ethylene glycol solution) on the particle size of the resulting PVP-protected Rh NPs (PVP–Rh NPs) were investigated. The nucleation rate of PVP–Rh NPs was controlled by the pH. The results obtained in this experiment were in good agreement with those of a theoretical calculation reported by Goia and co-workers.[183] The reaction temperature also strongly affected the nucleation rate of PVP–Rh NPs. Based on these findings, they selected the appropriate pH and reaction temperature conditions and fabricated size-controlled PVP–Rh NPs (1.6 ± 0.3, 2.7 ± 0.3, and 5.1 ± 0.5 nm). Each sample of PVP–Rh NPs was stirred in ethanol with a GaN:ZnO photocatalyst to induce cocatalyst adsorption. Then, PVP was removed from the NPs by calcination at 673 K (Fig. 10A). A transmission electron microscope (TEM) image of the calcined sample revealed that although slight aggregation occurred on

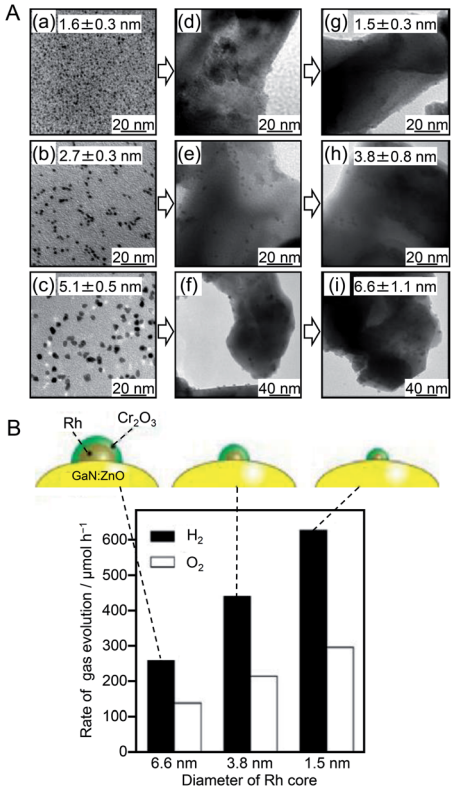

Fig. 10 (A) TEM images of three kinds of PVP–Rh NPs (a–c) as-synthesized, (d–f) adsorbed on GaN:ZnO, and (g–i) loaded on GaN:ZnO after calcination. (B) Initial rates of H_2 and O_2 evolution over GaN:ZnO modified with different-sized Cr_2O_3/Rh (shell/core) NPs. Black and white symbols/bars indicate H_2 and O_2, respectively. Reaction conditions: catalyst, 0.15 g; H_2SO_4 aq. (pH 4.5), 400 mL; light source, high-pressure Hg lamp (450 W) through an $NaNO_2$ aq. filter to cut UV light; reaction vessel, Pyrex inner-irradiation vessel. Reproduced with permission from ref. 183. Copyright 2013 American Chemical Society.

the GaN:ZnO photocatalyst, the Rh NPs still maintained their high monodispersity (1.5 ± 0.3, 3.8 ± 0.8, and 6.6 ± 1.1 nm). Then, a Cr_2O_3 layer was formed on the Rh NPs by photodeposition. Measurements of the water-splitting activity of the series of photocatalysts revealed that their water-splitting activity increased with decreasing cocatalyst size (Fig. 10B). They attributed this phenomenon to the following effects caused by the miniaturization of Rh NPs: (i) increased relative surface area of smaller Rh NPs; (ii) improved charge separation; and (iii) increased active sites for the HER.

The above examples demonstrated that control of the HER cocatalyst is an effective approach to improve the water-splitting activity of photocatalysts. In 2010, Domen *et al.*[184] showed that co-loading of an OER cocatalyst with an HER cocatalyst led to even higher water-splitting activity. In this study, GaN:ZnO was used as the photocatalyst, Cr_2O_3/Rh (shell/core) NPs were employed as the HER cocatalyst, and Mn_3O_4 NPs as the OER cocatalyst (Fig. 11A). First, MnO NPs (9.2 ± 0.4 nm) were

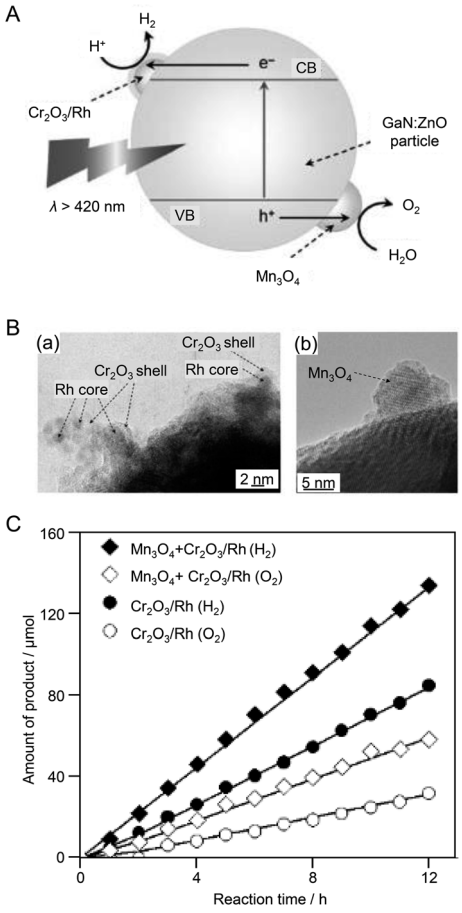

Fig. 11 (A) Proposed reaction mechanism for visible light-driven overall water splitting on GaN:ZnO modified with Mn_3O_4 and Cr_2O_3/Rh (shell/core) NPs. CB: conduction band, VB: valence band, e^-: electron, h^+: hole. (B) TEM images of GaN:ZnO modified with Mn_3O_4 and Cr_2O_3/Rh (shell/core) NPs: (a) Cr_2O_3/Rh NPs, (b) Mn_3O_4 NPs. (C) Time courses of H_2 and O_2 evolution using modified GaN:ZnO catalysts under visible light (λ > 420 nm). Mn loading: 0.05 wt%. Reproduced with permission from ref. 184. Copyright 2010 Wiley-VCH.

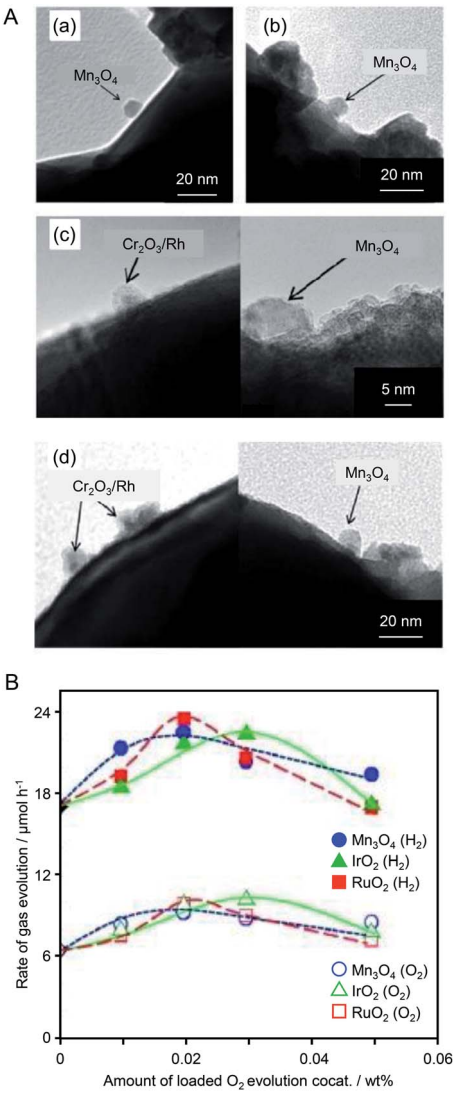

Fig. 12 (A) TEM images of (a and b) Mn_3O_4 NPs/GaN:ZnO and (c and d) Cr_2O_3/Rh NPs + Mn_3O_4 NPs/GaN:ZnO (a and c) before and (b and d) after calcination of the photocatalyst at 873 K. (B) Photocatalytic activity of GaN:ZnO co-loaded with different OER cocatalysts and Cr_2O_3/Rh NPs. Circles, triangles, and squares indicate the loading of Mn_3O_4, IrO_2, and RuO_2 NPs, respectively. Closed and open symbols denote H_2 and O_2, respectively. Reproduced with permission from ref. 185. Copyright 2014 Wiley-VCH.

synthesized by a liquid-phase reduction method as a precursor of the OER cocatalyst. The MnO NPs were adsorbed on the GaN:ZnO photocatalyst and then calcined at 673 K to form Mn_3O_4 NPs. Next, Cr_2O_3/Rh NPs were loaded on the GaN:ZnO photocatalyst as an HER cocatalyst. TEM measurements confirmed that the two types of cocatalysts were loaded on the photocatalyst without covering each other (Fig. 11B). The water-splitting activities of the photocatalyst loaded with only Cr_2O_3/Rh NPs and that loaded with both Cr_2O_3/Rh NPs and Mn_3O_4 NPs were measured. The results revealed that: (i) an HER cocatalyst (Cr_2O_3/Rh) is necessary for H_2 production; (ii) the photocatalyst co-loaded with both HER and OER cocatalysts (Cr_2O_3/Rh NPs and Mn_3O_4 NPs) showed higher activity than the

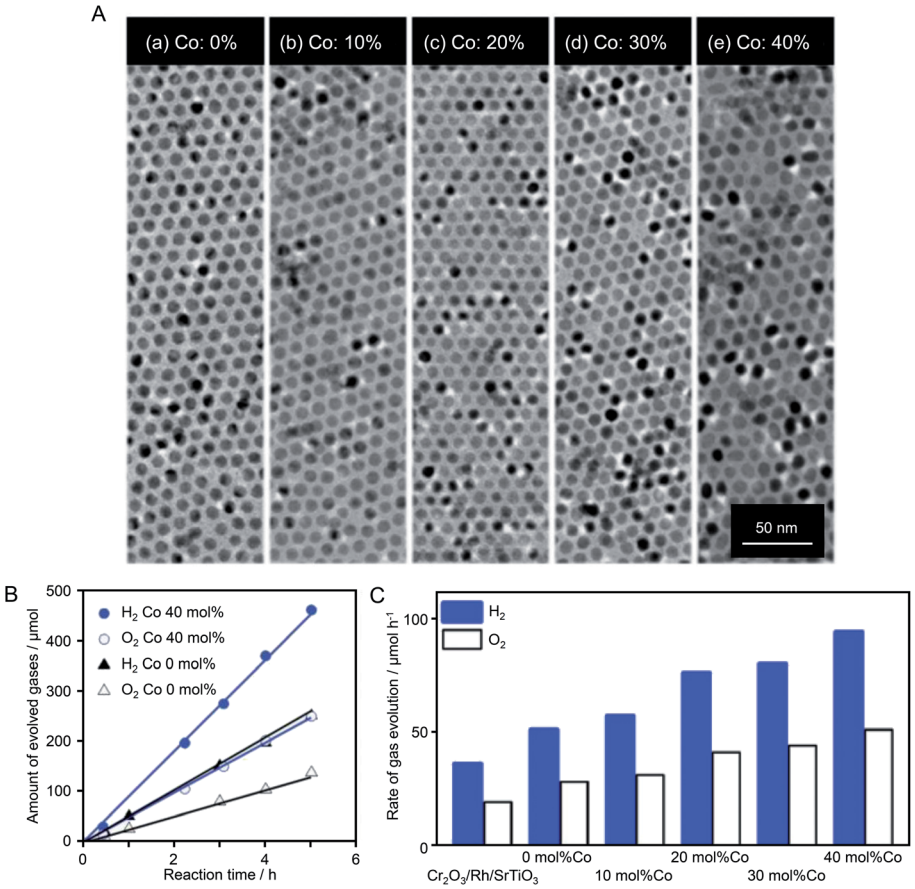

Fig. 13 (A) TEM images of $Co_xMn_{1-x}O$ NPs (~9 nm) with different Co ratios of (a) 0, (b) 10, (c) 20, (d) 30, and (e) 40 mol% Co. (B) Time course of overall water splitting using Cr_2O_3/Rh + $Co_xMn_{3-x}O_4$/$SrTiO_3$ under light irradiation (λ > 300 nm). The amount of loaded $Co_xMn_{3-x}O_4$ was 0.05 wt% calculated from the sum of Co and Mn. (C) Photocatalytic activities of Cr_2O_3/Rh/$SrTiO_3$ and Cr_2O_3/Rh + $Co_xMn_{3-x}O_4$/$SrTiO_3$ in overall water splitting. Co ratios were 0, 10, 20, 30, and 40 mol% Co. The loading amount was 0.05 wt%, as calculated from the sum of Co and Mn. Reaction conditions: catalyst, 0.1 g; aqueous solution, 100 mL; light source, 300 W Xe lamp (λ > 300 nm); reaction vessel, Pyrex top-irradiation vessel. Reproduced with permission from ref. 186. Copyright 2018 The Royal Society of Chemistry.

photocatalyst loaded with only the HER cocatalyst (Cr_2O_3/Rh NPs) (Fig. 11C); and (iii) water-splitting activity depended on the loading amount of OER cocatalyst (Mn_3O_4 NPs). It was noted that such a co-loading method of both HER and OER cocatalysts is also applicable to cases where NPs composed of different metals are used as cocatalysts.

Thus, control of the cocatalyst is effective for both the HER and OER. However, in the early stages of research on cocatalysts, it was unclear whether the HER or OER was the rate-limiting step in the water-splitting reaction. In 2014, Domen and colleagues conducted a study to determine the rate-limiting step of water splitting.[185] In this study, GaN:ZnO was again used as the photocatalyst, along with Mn_3O_4 NPs, RuO_2 NPs, or IrO_2 NPs as the OER cocatalyst and Cr_2O_3/Rh NPs as the HER cocatalyst (Fig. 12A). Evaluation of the water-splitting activity of each photocatalyst revealed that their activities were almost independent of the type of OER cocatalyst (Fig. 12B). Also, the amount of loaded OER cocatalyst to achieve high activity was much smaller than that of the HER cocatalyst. These results suggested that the HER was the rate-limiting step of water splitting by the photocatalyst used in this study. Based on these findings, they also optimized the HER cocatalyst. Specifically, GaN:ZnO photocatalysts co-loaded with RuO_2 NPs and Cr_2O_3/Rh NPs were fabricated by both liquid-phase adsorption of Rh NPs (3.3 ± 0.8 nm) and photodeposition of Rh NPs. They measured the water-splitting activities of both types of Cr_2O_3/Rh NPs + RuO_2 NPs/GaN:ZnO photocatalysts. The photocatalyst with Cr_2O_3/Rh NP cocatalyst loaded using liquid-phase adsorption showed higher water-splitting activity than that with the cocatalyst NPs loaded using the photodeposition method. These results indicate that controlling the HER cocatalyst is very important for enhancing the water-splitting activity of the GaN:ZnO photocatalyst.

When $SrTiO_3$ was used as the photocatalyst instead of GaN:ZnO solid solution, control of the OER cocatalyst also proved effective to improve water-splitting activity. In 2018, Teranishi *et al.*[186] synthesized $Co_xMn_{3-x}O_4$ NPs (Co/(Co + Mn) = 0–40 mol%) by doping Co into Mn_3O_4 NPs using a liquid-phase reduction method (Fig. 13A). The obtained $Co_xMn_{3-x}O_4$ NPs were loaded on an $SrTiO_3$ photocatalyst as OER cocatalysts after Cr_2O_3/Rh NPs were loaded as HER cocatalysts (Fig. 13B). TEM analysis confirmed that the particle size (~9 nm) of the Co_x-$Mn_{3-x}O_4$ NPs was maintained after loading on $SrTiO_3$. The water-splitting activity of the photocatalyst increased with the

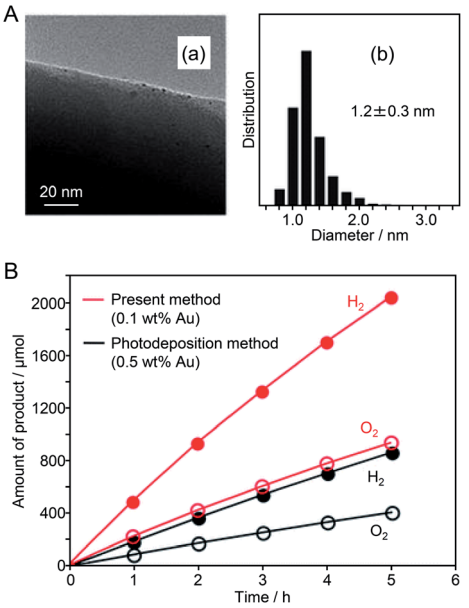

Fig. 14 (A) (a) TEM image and (b) size distribution of adsorbed NCs estimated from the TEM image of Au_{25} NC/$BaLa_4Ti_4O_{15}$. (B) Time course of water splitting over Au_{25} NC/$BaLa_4Ti_4O_{15}$ photocatalyst (0.1 wt% Au) prepared by the present method (red) and Au NPs/$BaLa_4Ti_4O_{15}$ photocatalyst (0.5 wt% Au) prepared by the conventional photodeposition method (black). Reaction conditions: photocatalyst, 0.5 g; distilled water, 350 mL; light source, high-pressure Hg lamp (400 W), inner irradiation cell made of quartz. Reproduced with permission from ref. 187. Copyright 2013 The Royal Society of Chemistry.

amount of Co of $Co_xMn_{3-x}O_4$. The photocatalyst loaded with $Co_xMn_{3-x}O_4$ NPs with a Co/(Co + Mn) ratio of 40 mol% showed water-splitting activity that was 1.8 times higher than that of the catalyst loaded with Mn_3O_4 NPs (Fig. 13B and C). To investigate the origin of such activity enhancement, they examined the electrocatalytic activity of $Co_xMn_{3-x}O_4$-loaded $BiVO_4$ photocatalysts in the OER. The results revealed that the efficiency of hole transfer from the photocatalyst to the cocatalyst was not increased by Co doping. Based on these results, they attributed the improvement of water-splitting activity to the increased OER activity on the cocatalyst surface induced by Co doping.

4.1.2. Use of atomically precise colloidal metal NCs. As shown in Section 4.1.1, using controlled colloidal metal NPs as a cocatalyst precursor can lead to photocatalysts with improved water-splitting activity. Among the metal NPs/NCs synthesized in the liquid phase, SR-protected metal NCs (metal = Au, Ag, Cu, *etc.*) can be synthesized with a particle size of about 1 nm.[82–107] If such ultrafine metal NCs are used as cocatalysts, it is expected that highly active water-splitting photocatalysts will be obtained based on the drastic increase in the surface atomic ratio of such small cocatalyst particles. In addition, it recently became possible to substitute some of the metal atoms of SR-protected metal NCs with a different element.[46–56] If these alloys NCs are used as cocatalyst precursors, it is expected that the effect of the chemical composition of the cocatalyst on the water-splitting activity of photocatalysts could be clarified at the atomic level, thereby providing clear design guidelines for the development of highly active photocatalysts.

Since 2013, Negishi's group has published several papers on the use of atomically precise metal NCs as precursors of HER cocatalysts. First, in 2013, they succeeded in loading Au_{25} NC with high dispersion on the surface of a UV light-responsive $BaLa_4Ti_4O_{15}$ photocatalyst.[187] In this experiment, first, Au_{25} NC protected by glutathionate (SG), $Au_{25}(SG)_{18}$, were synthesized precisely. Then, $Au_{25}(SG)_{18}$ was adsorbed on $BaLa_4Ti_4O_{15}$. Thereafter, the ligands of $Au_{25}(SG)_{18}$ were removed by calcination, providing Au_{25} NC-loaded $BaLa_4Ti_4O_{15}$ (denoted as Au_{25} NC/$BaLa_4Ti_4O_{15}$). Various evaluations of Au_{25} NC/$BaLa_4Ti_4O_{15}$ confirmed that the Au_{25} NCs were well dispersed on $BaLa_4Ti_4O_{15}$ (Fig. 14A), and that most of the ligands were removed by calcination. The water-splitting activity of Au_{25} NC/$BaLa_4Ti_4O_{15}$ was 2.6 times higher than that of $BaLa_4Ti_4O_{15}$ loaded with Au NPs with a diameter of 10–30 nm by the photodeposition method (this sample is denoted as Au NPs/$BaLa_4Ti_4O_{15}$) (Fig. 14B). These results indicate that the use of the fine Au NC cocatalyst is indeed effective for enhancing the water-splitting activity of the photocatalyst. In another paper, Negishi's group reported that such an improvement in water-splitting activity caused by the ultra-miniaturization of the Au cocatalyst also occurred when $SrTiO_3$ was used as a photocatalyst.[188] This result demonstrates that loading the fine Au NC cocatalyst (more widely metal NCs[120]) is also possible for the other photocatalysts when using SG as a ligand of NCs.

In 2015, Negishi's group synthesized a series of $Au_n(SG)_m$ NCs (n = 10, 15, 18, 25, and 39) with controlled numbers of constituent atoms with atomic precision and used the NCs as cocatalyst precursors.[189] They investigated the correlation between cocatalyst size and water-splitting activity. In this study, when $Au_n(SG)_m$ NCs (n = 22, 29, and 33) were used as precursors, the aggregation of Au NCs on the photocatalyst surface occurred during adsorption or calcination. It has been revealed that $Au_n(SG)_m$ NCs (n = 22, 29, and 33) are metastable species which are kinetically trapped during the NC formation and decompose (release of SG or Au-SG oligomers) in aqueous solution in a shorter time when compared with $Au_n(SG)_m$ NCs (n = 10, 15, 18, 25, and 39).[81] It was that for $Au_n(SG)_m$ NCs (n = 22, 29, and 33), part of the $Au_n(SG)_m$ NCs dissociate during the stirring process and Au-SG oligomers, formed from the dissociated products, adsorb conjunctively with the $Au_n(SG)_m$ NCs. The existence of such Au-SG oligomers was considered to promote cohesion of clusters on $BaLa_4Ti_4O_{15}$ during calcination. These results indicate that it is difficult to load $Au_n(SG)_m$ NCs that are unstable in solution on the $BaLa_4Ti_4O_{15}$ photocatalyst while maintaining the number of constituent atoms of NCs. This means that it is essential to use metal NCs that are stable in solution as a cocatalyst precursor to achieve precise loading of metal NCs (Fig. 15A). Then, the correlation between cocatalyst size and water-splitting activity was investigated by evaluating the water-splitting activities of Au_n NCs/$BaLa_4Ti_4O_{15}$ photocatalysts prepared using $Au_n(SG)_m$ NCs (n = 10, 15, 18, 25, and 39), which are stable in solution,[81] as cocatalyst precursors. It was found that the water-splitting activity increased as the size of the Au_n NC cocatalyst decreased (Fig. 15B). Because the

increase in activity with cocatalyst size decrease was modest, it was considered that the change in activity between the catalysts was mainly caused by the change in the proportion of Au NC surface atoms with miniaturization (*i.e.*, Au atoms that react with hydrogen). Conversely, the difference in water-splitting activity between Au_n NCs/$BaLa_4Ti_4O_{15}$ and Au NPs/$BaLa_4Ti_4O_{15}$ could not be fully explained by the difference in the number of surface atoms (Fig. 15B). From various analyses, it was found that the activity per Au atom on the surface of Au_{10} NCs/$BaLa_4Ti_4O_{15}$ was only about 15–25% of that of Au NPs/$BaLa_4Ti_4O_{15}$. Therefore, it was concluded that the main factor behind the improved activity caused by the ultra-miniaturization of the HER cocatalyst (Fig. 15B) was the increase of the number of surface Au atoms with an efficiency exceeding the decrease in activity per Au atom.

In the same paper, Negishi *et al.*[189] also examined the importance of ligand removal in such composite systems. Multiple studies have reported that for composites composed of $Au_n(SG)_m$ NCs and semiconductor photocatalysts, electron transfer occurs even when the ligands are present.[139] Indeed, $Au_{25}(SG)_{18}$ NC/$BaLa_4Ti_4O_{15}$ that had not been calcined showed higher water-splitting activity than that of $BaLa_4Ti_4O_{15}$ without the NC cocatalysts (Fig. 15C). This indicates that electron transfer occurs between the $Au_{25}(SG)_{18}$ NC and $BaLa_4Ti_4O_{15}$ without removing the ligands, and thus $Au_{25}(SG)_{18}$ NC also function as a cocatalyst. However, the water-splitting activity of $Au_{25}(SG)_{18}$ NC/$BaLa_4Ti_4O_{15}$ was about 23% of that of Au_{25} NC/$BaLa_4Ti_4O_{15}$ with the ligands removed (Fig. 15C). This means that the presence of the ligands lowers the efficiency of the electron transfer between Au_{25} NC and $BaLa_4Ti_4O_{15}$ or decreases the activity of individual Au atoms. These results clarified that ligand removal by calcination is very important to obtain composite photocatalysts with high water-splitting activity.

In this way, the use of the fine metal NCs as a cocatalyst is effective to improve the water-splitting activity of photocatalysts. However, the ORR, which is a reverse reaction of water splitting, proceeds simultaneously with the HER on the Au_{25} NC surface.[188] Therefore, to more effectively utilize the high surface area unique to fine metal NCs and thereby obtain highly active photocatalysts, it is necessary to form a shell that suppresses the ORR on the surface of Au_{25} NC. In 2018, Kurashige and co-workers attempted to form a Cr_2O_3 shell on Au_{25} NC.[190] In the case of the Cr_2O_3/Rh NPs described in Section 4.1, the Cr_2O_3 shell was formed by photodeposition. However, in the case of Au_{25} NC/$BaLa_4Ti_4O_{15}$, light irradiation induced the aggregation of Au_{25} NC on $BaLa_4Ti_4O_{15}$. Therefore, it was difficult to use

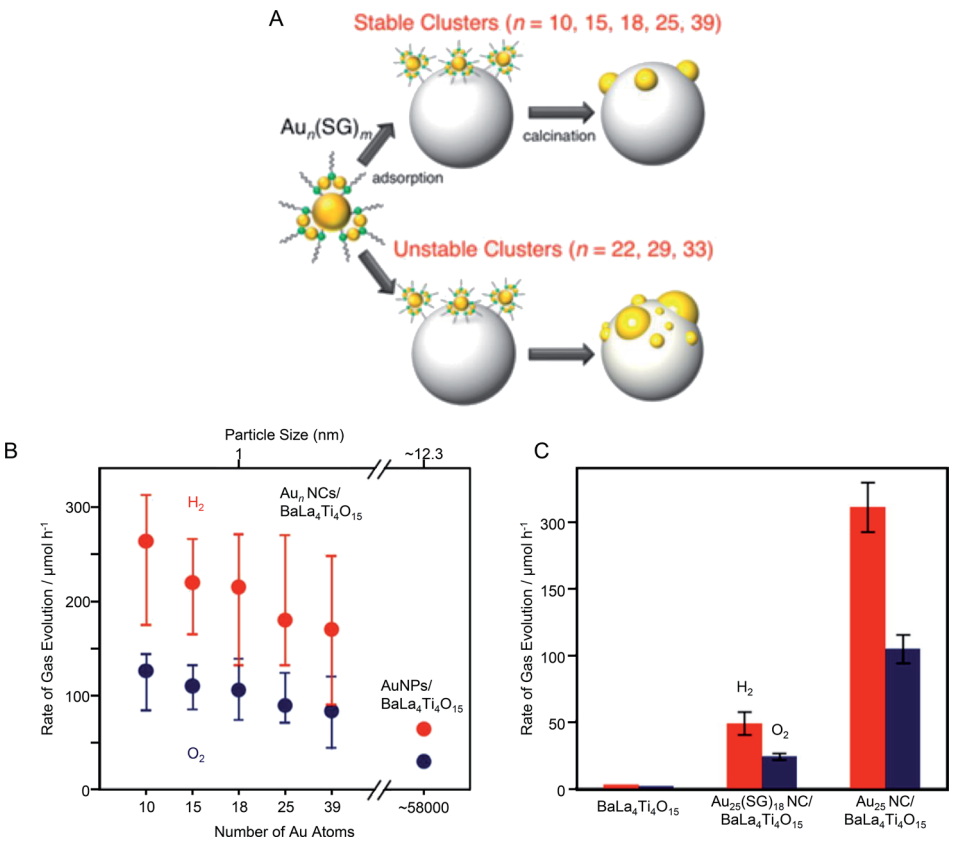

Fig. 15 (A) Schematic of the size control of Au_n NCs loaded on photocatalysts. (B) Effect of cluster size on water-splitting activity studied using Au_n NCs/$BaLa_4Ti_4O_{15}$ and Au NPs/$BaLa_4Ti_4O_{15}$ photocatalysts. The average values obtained from four measurements are plotted herein. (C) Comparison of the photocatalytic activities of $BaLa_4Ti_4O_{15}$, $Au_{25}(SG)_{18}$ NC/$BaLa_4Ti_4O_{15}$, and Au_{25} NC/$BaLa_4Ti_4O_{15}$. Reproduced with permission from ref. 189. Copyright 2015 American Chemical Society.

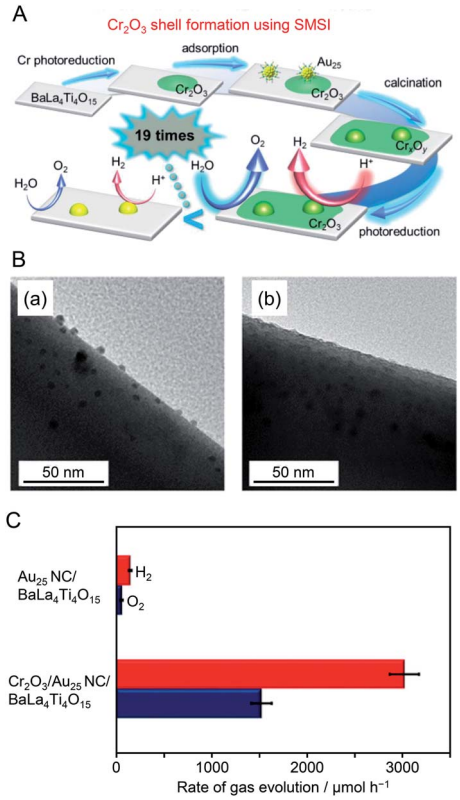

Fig. 16 (A) Schematic of the preparation of Cr_2O_3/Au_{25} NC/$BaLa_4Ti_4O_{15}$. (B) TEM images of (a) Au_{25} NC/$BaLa_4Ti_4O_{15}$ and (b) Cr_2O_3/Au_{25} NC/$BaLa_4Ti_4O_{15}$ after UV irradiation for 10 h. (C) Comparison of rates of H_2 and O_2 evolution by photocatalytic water splitting over Au_{25} NC/$BaLa_4Ti_4O_{15}$ and Cr_2O_3/Au_{25} NC/$BaLa_4Ti_4O_{15}$ (0.5 wt% Cr). Averages of values obtained from several experiments are shown. Reproduced with permission from ref. 190. Copyright 2018 American Chemical Society.

photodeposition to form a Cr_2O_3 shell on Au_{25} NC loaded on $BaLa_4Ti_4O_{15}$ while maintaining the size of the NCs.

Surface science research has revealed that when a metal oxide supporting metal NPs is heated under H_2 or O_2 atmosphere, a strong metal–support interaction (SMSI) is induced and thereby an oxide film is formed on the metal NPs.[191–194] Kurashige *et al.* attempted to use such an SMSI effect to form a Cr_2O_3 shell on the Au_{25} NC surface (Fig. 16A). Specifically, a Cr_2O_3 layer was deposited on $BaLa_4Ti_4O_{15}$ by photodeposition to form $Cr_2O_3/BaLa_4Ti_4O_{15}$ before loading Au_{25} NC (Fig. 16A). Then, $Au_{25}(SG)_{18}$ was adsorbed on $Cr_2O_3/BaLa_4Ti_4O_{15}$, and both ligand removal and surface protection by the SMSI effect were achieved by calcination. A TEM image of the photocatalyst after calcination showed the formation of a thin film with a thickness of about 0.7–0.9 nm around particles with a diameter of about 1 nm (Fig. 16B). This indicates that the Au_{25} NC were covered with a chromium oxide layer during calcination (Fig. 16A). Some of the chromium oxide layer of Cr_2O_3/Au_{25} NC/$BaLa_4Ti_4O_{15}$ was oxidized to a highly oxidized state during calcination. The photocatalyst was irradiated with UV light to reduce the highly oxidized chromium oxide to Cr_2O_3 and thereby the desired Cr_2O_3/Au_{25} NC/$BaLa_4Ti_4O_{15}$ was obtained. The water-splitting activity of Cr_2O_3/Au_{25} NC/$BaLa_4Ti_4O_{15}$ was about 19 time higher than that of Au_{25} NC/$BaLa_4Ti_4O_{15}$ (Fig. 16C). This indicates that the formation of the Cr_2O_3 shell is effective at suppressing the ORR on the surface of the Au NC cocatalyst. The formation of such a Cr_2O_3 shell also suppressed aggregation of the cocatalyst during light irradiation. This indicates that the Cr_2O_3 shell formed by the method established by Kurashige and colleagues improves not only the water-splitting activity but also the stability of the cocatalyst on the photocatalyst surface.

It is expected that photocatalysts with higher water-splitting activity could be realized by heteroatom doping of fine Au NC cocatalysts. In previous studies on the effect of heteroatom doping on photocatalyst activity, experiments have been conducted using photocatalysts with distributions of the particle size and doping ratio (chemical composition) of the cocatalysts.[195–201] To obtain a deep understanding of the effect of heteroatom doping on photocatalytic activity and thereby establish clear design guidelines for photocatalyst activation, it is essential to study composite photocatalysts on which the cocatalysts have strictly controlled chemical composition. Recently, Kurashige *et al.*[202] attempted to use $Au_{24}Pd$ and $Au_{24}Pt$ NCs, in which one Au atom of the Au_{25} NC is substituted with Pd or Pt, as an HER cocatalyst. $Au_{24}Pd(SR)_{18}$ and $Au_{24}Pt(SR)_{18}$ NCs can be precisely synthesized only when a hydrophobic ligand is used.[202] However, the metal NCs protected by hydrophobic ligands could not strongly interact with the hydrophilic surface of $BaLa_4Ti_4O_{15}$, which led to poor adsorption on the photocatalyst. Then, they replaced some of the ligands of $Au_{24}Pd(SR)_{18}$ and $Au_{24}Pt(SR)_{18}$ NCs with a hydrophilic ligand, which allowed them to adsorb on $BaLa_4Ti_4O_{15}$ at a high adsorption rate (Fig. 17A). The ligands on the NC surface were removed by calcination (Fig. 17A).

Investigation of the photocatalyst loaded with cocatalyst NCs controlled with atomic precision revealed the following three points about the heteroatom doping of the Au cocatalyst: (i) the Pd atom was located on the surface of the metal NC and the Pt atom was located at the interface between the metal NC and photocatalyst (Fig. 17B); (ii) Pd doping induced a decrease of water-splitting activity and Pt doping caused water-splitting activity to increase (Fig. 17C); (iii) these opposite effects of Pd and Pt heteroatom doping are strongly related to the location of the doped heteroatom (Fig. 17B). The results also showed that combining Pt doping and surface protection of the cocatalyst with a Cr_2O_3 shell increased the activity and stability of the photocatalysts to a greater extent than only Pt doping (Fig. 17D).

In the above series of research, Au was used as the base element of the NC cocatalyst. It has been predicted that Rh has higher catalytic activity than Au with respect to the HER based on volcano plots for hydrogen adsorption and desorption.[203] Therefore, it is expected that a highly active water-splitting photocatalyst could be obtained by loading Rh and Cr oxide NPs/NCs as an HER cocatalyst on the photocatalyst. Indeed, Domen and co-workers reported that a photocatalyst loaded with Rh(III)–Cr(III) mixed oxide NPs ($Rh_{2-x}Cr_xO_3$; particle size = 10–30 nm) showed higher water-splitting activity than that of photocatalysts loaded with metal NPs composed of other elements.[204–207] If ultrafine $Rh_{2-x}Cr_xO_3$ NCs could be loaded on

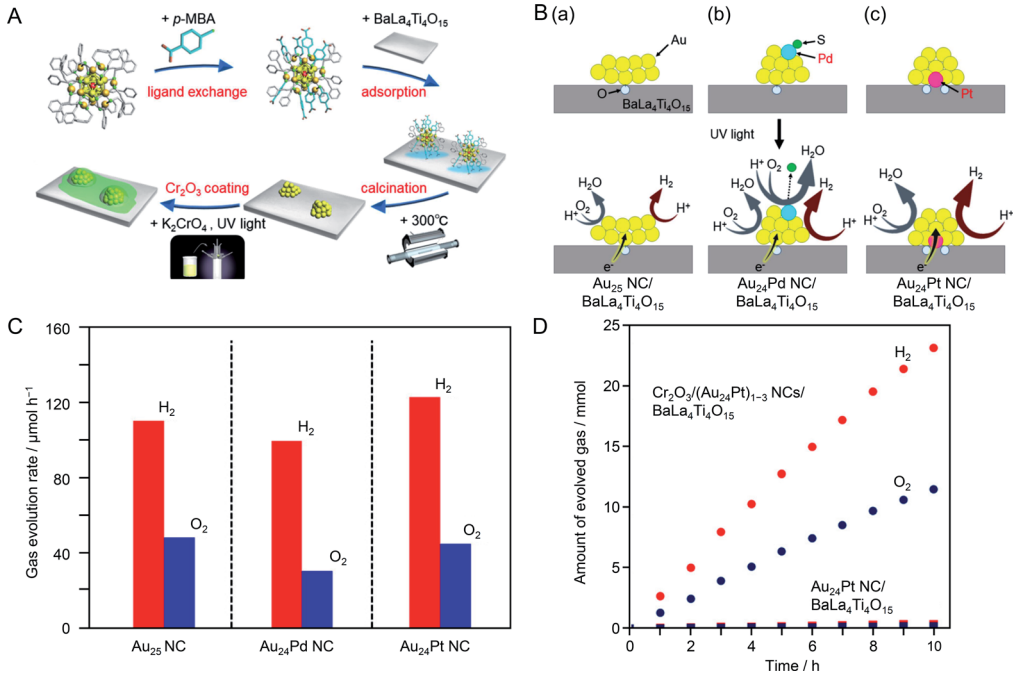

Fig. 17 (A) Schematic of the experimental procedure. (B) Proposed structures of $Au_{24}M$ NC/$BaLa_4Ti_4O_{15}$ with M of (a) Au, (b) Pd, and (c) Pt before (upper) and during (lower) the water-splitting reaction. (C) Rates of photocatalytic evolution of H_2 and O_2 by water splitting over $Au_{24}M$ NC/$BaLa_4Ti_4O_{15}$ with M of Au, Pd, and Pt. (D) Time course of water splitting over $Cr_2O_3/(Au_{24}Pt)_{1-3}$ NCs/$BaLa_4Ti_4O_{15}$ and $Au_{24}Pt$ NC/$BaLa_4Ti_4O_{15}$. Reproduced with permission from ref. 202. Copyright 2019 American Chemical Society.

the photocatalyst as an HER cocatalyst, it might be possible to activate the photocatalyst further. Very recently, Kurashige *et al.*[208] attempted to load fine $Rh_{2-x}Cr_xO_3$ NCs as an HER cocatalyst on $BaLa_4Ti_4O_{15}$ by modifying the method shown in Fig. 16A. Unfortunately, the precise synthesis of $Rh_{2-x}Cr_xO_3$ NCs has not been reported. Therefore, in this experiment, a complex containing $Rh_2(SG)_2$ as the main component was used as a precursor. First, $Rh_2(SG)_2$ was adsorbed on $BaLa_4Ti_4O_{15}$ covered with a Cr_2O_3 film, and then the resulting photocatalyst was calcined. These operations resulted in loading of $Rh_{2-x}Cr_xO_3$ NCs on the photocatalyst (Fig. 18A). Various structural analyses showed that about six $Rh_2(SG)_2$ complexes aggregated during adsorption and that the Rh and Cr_2O_3 films formed solid solutions during calcination (Fig. 18B). Monodisperse $Rh_{2-x}Cr_xO_3$ NCs with a particle size of 1.3 ± 0.3 nm were loaded on $BaLa_4Ti_4O_{15}$ by this method (Fig. 18C). The obtained photocatalyst exhibited an apparent quantum yield of 16% under 270 nm excitation, which is the highest achieved for $BaLa_4Ti_4O_{15}$ to date (Fig. 18D). These results indicate that loading $Rh_{2-x}Cr_xO_3$ NCs by this method is an effective approach to improve the water-splitting activity of the $BaLa_4Ti_4O_{15}$ photocatalyst. In principle, this method is applicable to the other photocatalysts. $Rh_{2-x}Cr_xO_3$ has already proved a useful cocatalyst in many water-splitting photocatalysts.[204–207,209,210] In the future, it is expected that high quantum yields can be achieved for many water-splitting photocatalysts using this technique.

In the above research, the Cr_2O_3 shell on the cocatalyst surface suppressed the ORR, which is one of the reverse reactions of water splitting. When Pt NPs were used as a cocatalyst, the hydrogen oxidation reaction (HOR), which is also a reverse reaction of water splitting, proceeds simultaneously with the HER. In 2013, Wang and colleagues showed that platinum oxide (PtO) NCs could suppress the HOR.[211] In their study, UV-responsive TiO_2 was used as the photocatalyst and PtO or Pt NCs were used as the HER cocatalyst. To load PtO NCs on the photocatalyst, $TiO_2\{001\}$ nanosheets and poly(methacrylic acid) were dispersed in an aqueous solution containing chloroplatinic acid. Fine PtO NCs were loaded on TiO_2 by injecting an aqueous solution of $NaBH_4$ into the vigorously stirring reaction solution to form PtO NCs/TiO_2.[212] The polymer in PtO NCs/TiO_2 was removed by washing the sample with ethanol several times. Pt NCs were loaded on TiO_2 to form Pt NCs/TiO_2 using the same mixing method without polymer. Scanning TEM (STEM) images revealed that the loaded PtO NCs (Fig. 19A) and Pt NCs had particle diameters of 1.0 ± 0.3 and 2.0 ± 0.5 nm, respectively. The HER and HOR activities of the obtained photocatalysts were evaluated (Fig. 19B). It was revealed that PtO NCs/TiO_2 showed high HER activity and suppressed HOR activity. Similar HOR suppression was not observed for Pt NCs/TiO_2 (Fig. 19B). To clarify the reasons for this difference, they conducted density functional theory (DFT) calculations using Pt_8O_8/TiO_2 and Pt_{12}/TiO_2 as models (Fig. 19C). The results revealed that the reaction between H and O occurred easily on Pt_{12}/TiO_2 because the adsorption energies of Pt–H and Pt–O were large. Conversely, for Pt_8O_8/TiO_2, it was shown that it was difficult for the HOR to occur because the adsorption energies of H and O were smaller than those of Pt_{12}/TiO_2

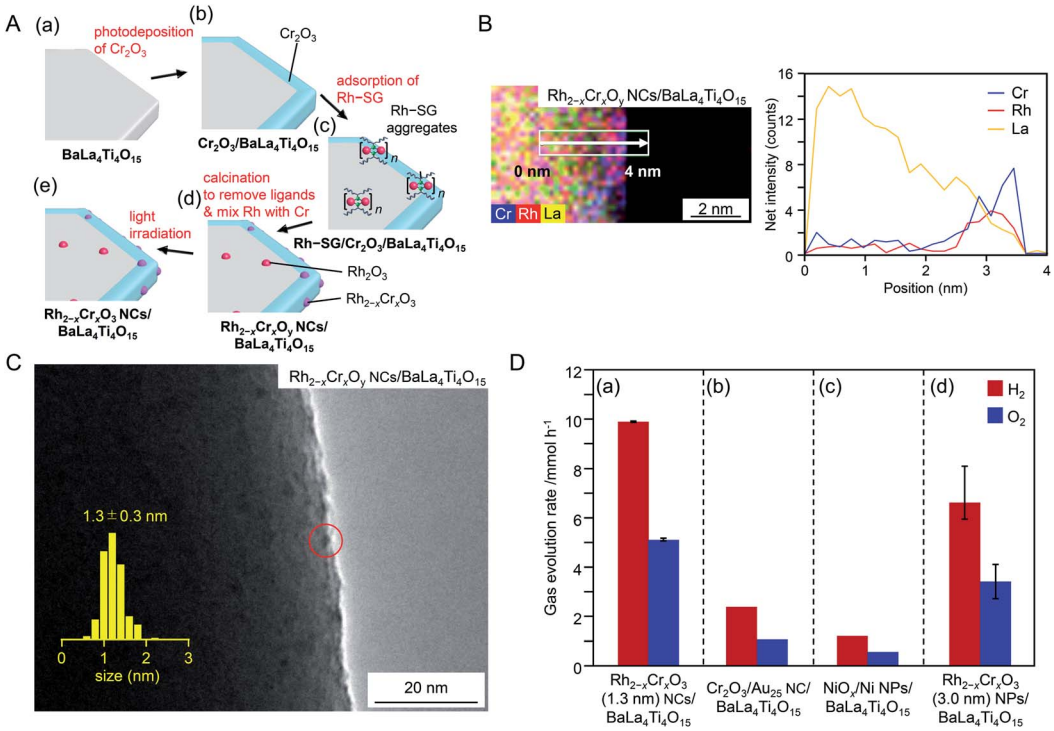

Fig. 18 (A) Schematic of the experimental procedure to form (a) $BaLa_4Ti_4O_{15}$, (b) $Cr_2O_3/BaLa_4Ti_4O_{15}$, (c) Rh–SG/$Cr_2O_3/BaLa_4Ti_4O_{15}$, (d) $Rh_{2-x}Cr_xO_y$ NCs/$BaLa_4Ti_4O_{15}$, and (e) $Rh_{2-x}Cr_xO_3$ NCs/$BaLa_4Ti_4O_{15}$. $Rh_{2-x}Cr_xO_y$ NCs indicates $Rh_{2-x}Cr_xO_3$ NCs including highly oxidized Cr (>+3). (B) Elemental mapping line analysis by STEM measurements for $Rh_{2-x}Cr_xO_y$ NCs/$BaLa_4Ti_4O_{15}$. (C) TEM image of $Rh_{2-x}Cr_xO_y$ NCs/$BaLa_4Ti_4O_{15}$. The red circles indicate the $Rh_{2-x}Cr_xO_3$ NCs. (D) Comparison of gas evolution rates over different photocatalysts (a) $Rh_{2-x}Cr_xO_3$ (1.3 nm) NCs/$BaLa_4Ti_4O_{15}$ (0.09 wt% Rh and 0.10 wt% Cr), (b) Cr_2O_3/Au_{25} NC/$BaLa_4Ti_4O_{15}$ (0.10 wt% Au and 0.50 wt% Cr), (c) NiO_x/Ni NPs/$BaLa_4Ti_4O_{15}$ (0.50 wt% Ni), and (d) $Rh_{2-x}Cr_xO_3$ (3.0 nm) NPs/$BaLa_4Ti_4O_{15}$ (0.10 wt% Rh and 0.15 wt% Cr). Reproduced with permission from ref. 208. Copyright 2020 Wiley-VCH.

(Fig. 19D). In this study, because PtO NCs were synthesized and loaded on TiO_2 in a single reaction system, it is difficult to judge whether size-controlled PtO NCs were synthesized and subsequently loaded on TiO_2 or the size of PtO NCs loaded on TiO_2 was controlled by the coexistence of polymer. In addition, the number of constituent atoms of the PtO and Pt NCs was not controlled with atomic precision. However, this study is important because it revealed a different approach to inhibit reverse reactions of water splitting.

In this way, the use of metal NCs with controlled fine size as a cocatalyst can induce an increase in water-splitting activity because of their large surface area. Such precisely controlled cocatalysts make it possible to obtain a deep understanding of the effects of cocatalyst size and heteroatom doping on photocatalyst activity, as well as the origins of these effects. The findings obtained from these studies are expected to lead to clear design guidelines for the development of highly active and stable water-splitting photocatalysts.

4.1.3. Use of other controlled NPs/NCs. Finally, we introduce an example in which the particle size of the cocatalyst of the water splitting photocatalyst was successfully controlled by a method other than the liquid-phase adsorption method. In 2015, Maeda *et al.* succeeded in loading fine Pt NCs (<1 nm) relatively monodispersely between an anionic nanosheet layers of $KCaNb_3O_{10}$ by adsorbing cationic Pt complexes ($[Pt(NH_3)_4]Cl_2 \cdot H_2O$) on the surface of an anionic nanosheet by electrostatic interaction and then conducting the hydrogen reduction on the resulting sample (intercalation method).[213] Pt NCs/$KCa_2Nb_3O_{10}$ obtained by this method showed higher water-splitting activity than Pt NCs/$KCa_2Nb_3O_{10}$ prepared by the impregnation method and RuO_2 NPs/$KCa_2Nb_3O_{10}$ fabricated by the intercalation method. It was interpreted that the Pt NCs were loaded monodispersely between the nanosheets because it was difficult for the formed Pt NCs to aggregate between the nanosheets due to steric hindrance. In this way, the control of the particle size of the cocatalyst by a method other than the liquid-phase adsorption method has also been progressing in recent years.

4.2. Application in H_2 evolution

In addition to the studies on overall water splitting described in Section 4.1, many reports on the improvement of the activity of each half reaction of water splitting (HER and OER) by controlling the cocatalyst have appeared recently. In the following subsections, we focus on research of HER using controlled colloidal metal NPs/NCs and introduce some typical research examples. The photocatalysts used in these studies are also summarized in Fig. 7. The materials and conditions used in the experiments are summarized in Table 2.

4.2.1. Use of colloidal metal NPs. Metal NPs have different electronic states and surface energies depending on the crystal

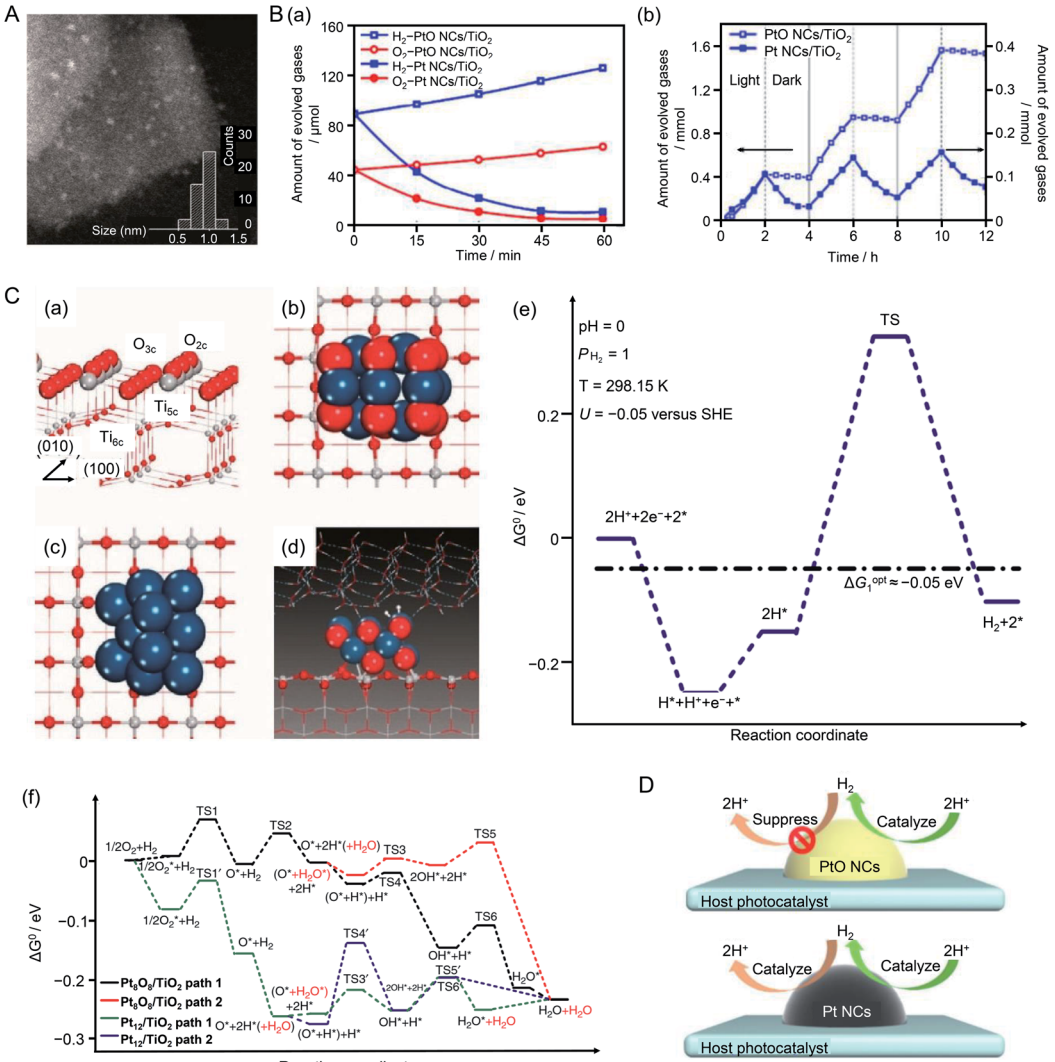

Fig. 19 (A) Representative STEM image clearly showing isolated three-dimensional PtO NCs (bright spots). (B) (a) Reaction time profiles of the HOR with H_2 and O_2 on PtO NCs/TiO_2 and Pt NCs/TiO_2 photocatalysts under UV-visible light irradiation ($\lambda > 300$ nm). (b) H_2 evolution and undesirable oxidation in methanol aqueous solution during three cycles of light irradiation ($\lambda > 300$ nm, 2 h) followed by dark conditions (light off, 2 h) on PtO NCs/TiO_2 and Pt NCs/TiO_2. (C) (a) Structure of the anatase TiO_2(001) surface. (b) Optimized Pt_8O_8 NCs adsorbed on the TiO_2(001) surface (Pt_8O_8 NCs/TiO_2) and (c) optimized Pt_{12} NCs/TiO_2. (d) Transition state structure of H*–H* coupling on Pt_8O_8 NCs/TiO_2 in the liquid phase, which contained two layers of water molecules above the Pt_8O_8 NCs. (e) Standard Gibbs free energy profile of the HER in aqueous solution on Pt_8O_8 NCs/TiO_2. (f) Standard Gibbs free energy profile of H_2 reacting with O_2 on Pt_8O_8 NCs/TiO_2 and Pt_{12} NCs/TiO_2 surfaces in the gas phase. Dark blue, gray, white, and red balls represent Pt, Ti, H, and O atoms, respectively. (D) Both PtO NCs and m-Pt NCs cocatalysts acted as H_2 evolution sites on the host photocatalyst surface. The undesirable H_2 reverse-reaction was suppressed by the PtO NC cocatalyst but facilitated by the Pt NC cocatalyst. Reproduced with permission from ref. 211. Copyright 2013 Nature Publishing Group.

face. Therefore, the adsorption of NPs on a substrate differs depending on the crystal face, and thereby the activity of the metal NPs also varies depending on the exposed crystal face. In 2013, Lu *et al.*[214] showed that controlling such crystal faces indeed led to changes in photocatalytic activity. In their study, UV-responsive TiO_2 was used as a photocatalyst. First, cubic-shaped Pt{100} NPs (4.7 ± 1.6 nm), hexagonal-shaped Pt{100/111} NPs (6.0 ± 1.5 nm), and tetrahedral-shaped Pt{111} NPs (6.5 ± 2.0 nm) were synthesized (Fig. 20A). Each type of Pt NPs was adsorbed on TiO_2 by stirring the Pt NPs with TiO_2 in water. In a series of photocatalytic HER activity measurements, the photocatalyst using Pt{111} NPs as the cocatalyst showed the highest HER activity (Fig. 20B and C). Pt{111} NPs have a higher percentage of Pt atoms at the corners and edges than is the case for Pt{100} NPs and Pt{100/111} NPs. Therefore, the apparent activation energy of Pt{111} NPs for H_2 generation is low (Fig. 20D). In addition, the Pt{111} NPs contain many active sites. It was considered that these reasons led to the rapid progress of the HER on the Pt{111} NP surface. Model calculations showed that it was easier to form H_2 molecules *via* bonding of each hydrogen atom on the Pt{111} NP cocatalyst

Table 2 Materials and experimental conditions in the study using liquid-phase adsorption method for hydrogen production (half reaction)

	Cocatalyst					
Semiconductor	Kinds	Loading amount	Size	Light source	Reactant solution	Ref.
TiO_2	Pt NPs {100}	0.5 wt%	4.7 ± 1.6 nm	300 W Xe lamp (λ > 420 nm)	15% (v/v) TEOA aq. with Eosin Y	214
	Pt NPs {100/111}	0.5 wt%	6.0 ± 1.5 nm			
	Pt NPs {111}	0.5 wt%	6.5 ± 2.0 nm			
TiO_2	Au NPs {100}	0.5 wt%	9.2 nm	300 W Xe lamp (λ > 420 nm)	15% (v/v) TEOA aq. with Eosin Y	215
	Au NPs {100/111}	0.5 wt%	9.5 nm			
	Au NPs {111}	0.5 wt%	8.5 nm			
g-C_3N_4	Rh NPs	0.25 wt%	4.1 ± 0.8 nm	Xe lamp (420 < λ < 630 nm)	10% methanol aq.	216
		0.23 wt%	5.9 ± 1.1 nm			
		0.34 wt%	7.8 ± 1.4 nm			
		0.27 wt%	9.1 ± 1.7 nm			
g-C_3N_4/ $Al_2Si_2O_5(OH)_4$	$Ni(OH)_2$ NPs	1 wt%	<100 nm	300 W Xe lamp (λ > 400 nm)	10 vol% methanol aq.	217
CdS	Pt–Pd NPs {100} (Pt : Pd = 2 : 1)	0.5 wt%	7.9 nm	300 W Xe lamp (λ > 420 nm)	1.0 M $(NH_4)_2SO_3$ aq.	218
	Pt–Pd NPs {111} (Pt : Pd = 2 : 1)	0.5 wt%	5.2 nm			
TiO_2 nanotubes	CuO NPs (A–C)	Cu/Ti ratio: 9 atom%	3 nm	400 W Hg lamp	10 vol% methanol aq.	219
	CuO NPs (WI)	Cu/Ti ratio: 9.6 atom%				
CdS	Pt NCs	1 wt%	0.9 ± 0.1 nm	300 W Xe lamp (λ > 420 nm)	Na_2S and Na_2SO_3 aq.	220
	Pt NPs	1 wt%	5 nm			
g-C_3N_4	Ag_{25}	0.2 wt%	1.5 ± 0.25 nm	Visible light (λ > 420 nm)	10 vol% TEOA aq.	221
	$PtAg_{24}$	0.2 wt%	1.5 ± 0.25 nm			
g-C_3N_4	Au_{25}	0.18 wt%		Visible light (λ > 420 nm)	10 vol% TEOA aq.	224
		0.49 wt%				
		0.96 wt%				
ZIF-8/TiO_2	Au_{25} Re complex		1.2 nm	300 W Xe lamp (λ > 420 nm)	H_2O (1 mL), TEOA (1 mL), acetonitrile (4 mL), $[Ru(bpy)_3]Cl_2 \cdot 6H_2O$ (10.0 μmol)	225
	Au NPs Re complex		~10 nm			

surface than was the case on the Pt{100} NPs and Pt{100/111} NPs.

In 2014, Lu's group also conducted similar research using Au NPs.[215] In this experiment, first, cubic-shaped Au{100} NPs, truncated cubic-shaped Au{100/111} NPs, and octahedral-shaped Au{111} NPs were synthesized by liquid-phase reduction. Each type of Au NPs was adsorbed on TiO_2 by stirring the Au NPs and TiO_2 in water. A series of photocatalytic HER activity measurements revealed that the photocatalyst using Au{111} NPs as a cocatalyst (denoted as Au{111} NPs/TiO_2) possessed the highest HER activity of the samples. Photoluminescence measurements and model calculations indicated that Au{111} NPs/TiO_2 showed high HER activity because of the same reasons as Pt{111} NPs/TiO_2.

As shown in the above examples, to control the cocatalyst, it is very important to select an appropriate element, refine the particle size, improve the dispersibility, form an alloy, form a shell to suppress reverse reactions of water splitting, and control shell thickness. In 2014, Hensen *et al.*[216] showed that the valence state of the Rh NP surface had also a large effect on the HER activity of a complex system composed of Rh NPs and visible light-responsive g-C_3N_4 photocatalyst. They synthesized PVP–Rh NPs with sizes of 4.1 ± 0.8, 5.9 ± 1.1, 7.8 ± 1.4, and 9.1 ± 1.7 nm and adsorbed them on g-C_3N_4 to form PVP–Rh NPs/g-C_3N_4 (Fig. 21A). Then, PVP on the Rh NP surface was removed by ozone oxidation. In general, removal of the protective ligand induces an increase in HER activity. However, the Rh NPs/g-C_3N_4 samples obtained after ozone oxidation showed lower HER activity than PVP–Rh NPs/g-C_3N_4 (Fig. 21B). When the samples after ozone oxidation were calcined under H_2 flow, their activity increased. These results indicated that the activity decreased when the surface of the Rh NP cocatalyst was oxidized by ozone, whereas the activity increased when the Rh NPs were reduced by calcination under flowing H_2. Thus, it was clarified that the high metallicity of the cocatalyst surface is important to improve the HER activity of Rh NPs/g-C_3N_4 photocatalysts.

Recently, Hojamberdiev *et al.*[217] also studied the HER activity of g-C_3N_4. In their study, $Ni(OH)_2$, which is a relatively inexpensive HER cocatalyst, and halloysite ($Al_2Si_2O_5(OH)_4$) as a hole trapping agent were co-loaded on g-C_3N_4 (Fig. 22A). The HER activity of the obtained photocatalyst was measured in an aqueous solution containing 10 vol% methanol as a sacrificial agent. The HER activity of the catalyst loaded with 1 wt% $Ni(OH)_2$ was about 40 times higher than that of g-C_3N_4 alone. This indicates that co-loading $Ni(OH)_2$ and halloysite is an effective approach to improve the HER activity of g-C_3N_4. $Ni(OH)_2$ loaded on a photocatalyst promoted charge separation by capturing photoexcited electrons, and the negative charges

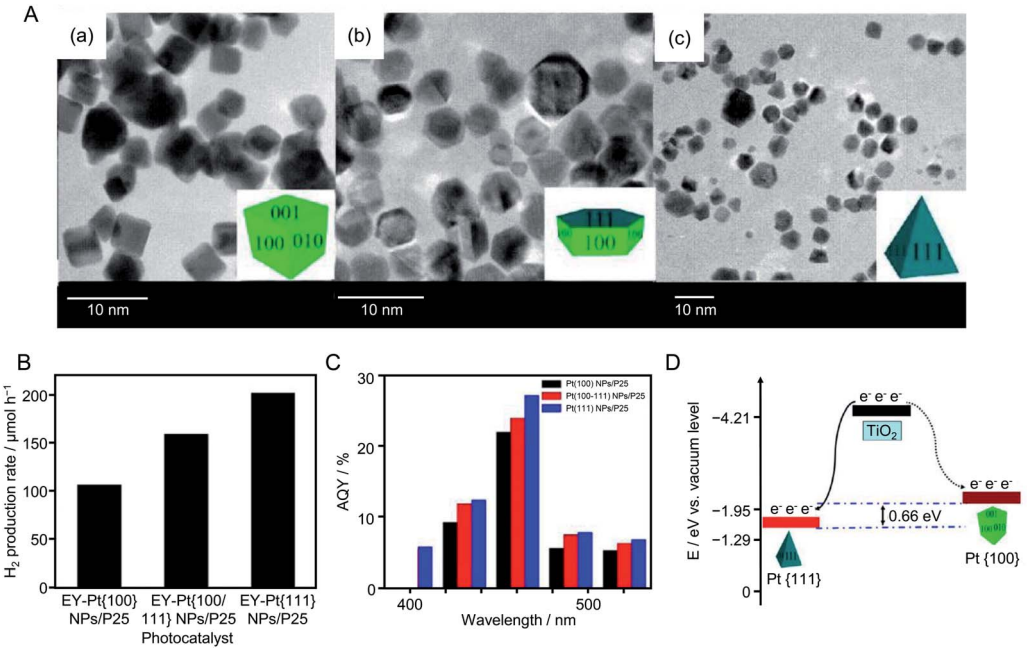

Fig. 20 (A) TEM images of (a) Pt{100}, (b) Pt{100/111}, and (c) Pt{111} NPs, respectively. The insets are schematics of the corresponding Pt NPs. (B) H_2 evolution rates of Eosin Y (4.0×10^{-4} M)-sensitized Pt{100} NPs/TiO_2, Pt{100/111} NPs/TiO_2, and Pt{111} NPs/TiO_2 photocatalysts from 100 mL of 15% (v/v) TEOA aqueous solution under visible light irradiation ($\lambda > 420$ nm). (C) Apparent quantum yield of the HER for the above three photocatalysts. Light source: 300 W Xe lamp with either a cut-off filter of 420 nm or band-pass filter. (D) Schematic of the different energy levels of Pt{100} (solid curve) and Pt{111} (dotted curve) facets. Reproduced with permission from ref. 214. Copyright 2013 American Chemical Society.

on the halloysite surface captured holes generated by photoexcitation. This behavior led to the extremely high HER activity of the catalyst co-loaded with $Ni(OH)_2$ and halloysite (Fig. 22B). A model calculation was performed to evaluate the adsorption affinity of water and methanol molecules on the catalyst surface. The results showed that the combination of g-C_3N_4, halloysite, and $Ni(OH)_2$ promoted the adsorption of water and methanol on the cocatalyst surface.

In the above research on HER cocatalysts, mono-metal NPs were used. In 2016, Yao and colleagues reported a study using alloy NPs as a cocatalyst.[218] In this study, visible light-responsive CdS was used as the photocatalyst and Pt–Pd alloy NPs were used as the cocatalyst. The loaded Pt–Pd NPs were Pt–Pd nanocubes with an {100} crystal plane (Fig. 23A) and Pt–Pd nano-octahedra with the {111} crystal plane. Both types of NPs were synthesized with multiple compositions (Pt : Pd = 1 : 1, 2 : 1, 3 : 1, and 1 : 2). The HER activity of the obtained photocatalysts was measured in aqueous solutions containing ammonium sulfite as a sacrificial agent. The catalyst loaded with Pt–Pd NPs with a Pd : Pt ratio of 2 : 1 showed the highest activity. This finding was attributed to the optimized hydrogen adsorption/desorption energy on the cocatalyst surface with a Pt : Pd ratio of 2 : 1. In addition, comparison of cocatalysts with different crystal planes revealed that the Pt–Pd nanocubes

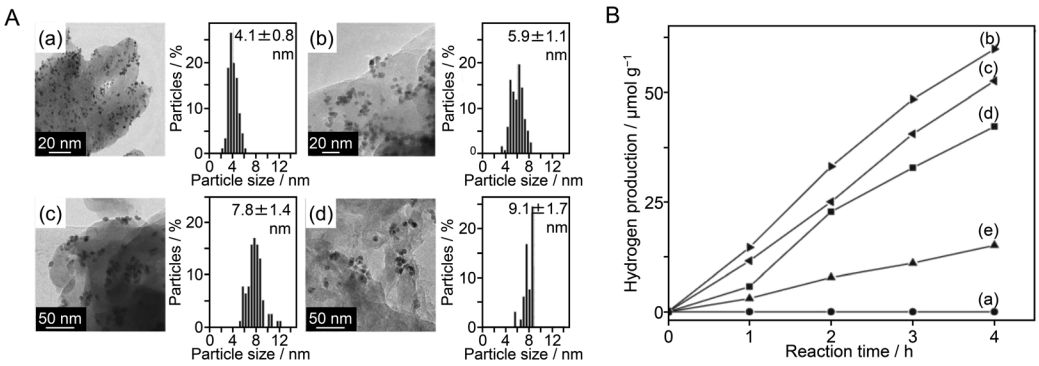

Fig. 21 (A) Representative TEM images and particle size distributions of (a) PVP–Rh (4.1 nm) NPs/g-C_3N_4, (b) PVP–Rh (5.9 nm) NPs/g-C_3N_4, (c) PVP–Rh (7.8 nm) NPs/g-C_3N_4 and (d) PVP–Rh (9.1 nm) NPs/g-C_3N_4. (B) Photocatalytic hydrogen production rates as a function of time for (a) pure g-C_3N_4, (b) PVP–Rh (4.1 nm) NPs/g-C_3N_4, (c) PVP–Rh (5.9 nm) NPs/g-C_3N_4, (d) PVP–Rh (7.8 nm) NPs/g-C_3N_4 and (e) PVP–Rh (9.1 nm) NPs/g-C_3N_4. Reproduced with permission from ref. 216. Copyright 2014 Elsevier Ltd.

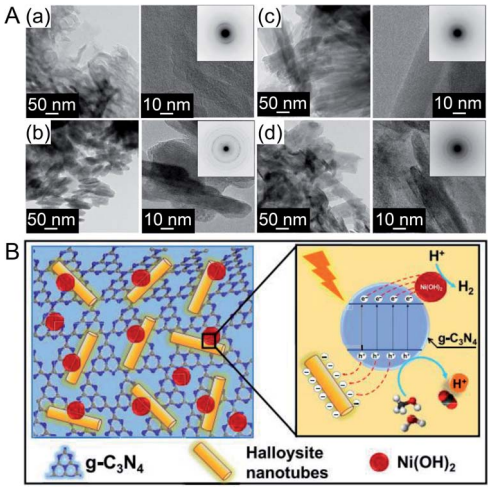

Fig. 22 (A) TEM and high-resolution TEM images of (a) g-C_3N_4, (b) $Ni(OH)_2$, (c) halloysite, and (d) $Ni(OH)_2$/g-C_3N_4 halloysite nanocomposites prepared with 1 wt% $Ni(OH)_2$. (B) Schematic representation of the separation and transfer of photogenerated charge carriers involved in photocatalytic H_2 evolution over the developed nanocomposite. Reproduced with permission from ref. 217. Copyright 2019 Elsevier Ltd.

with the {100} crystal plane had higher activity than that of the Pt–Pd nano-octahedra with the {111} crystal plane (Fig. 23B). The {100} crystal plane has a lower atomic density than that of the {111} crystal plane. They interpreted that the Pt–Pd nanocubes showed higher activity than the Pt–Pd nano-octahedra because the electron transfer from the photocatalyst to the cocatalyst occurred more efficiently on the {100} crystal plane than on the {111} crystal plane due to the lower atomic density of the former than the latter.

The shape and crystal plane of the photocatalyst also affect HER activity. In 2011, Sun *et al.*[219] reported that the HER activity of TiO_2 was improved when its morphology was modified to form cylindrical TiO_2 nanotubes (TNT) (Fig. 24A(a)). In this study, CuO NPs were used as an HER cocatalyst. CuO NPs were loaded on TiO_2 and TNT by adsorption and calcination (denoted as A–C; this is the same as liquid-phase adsorption) using $Cu(NO_3)_2$ as a precursor to form CuO NPs(A–C)/TiO_2 and CuO NPs(A–C)/TNT, respectively (Fig. 24A(b)). For comparison, CuO NPs were also loaded on TiO_2 and TNT by wet impregnation (WI) to give CuO NPs(WI)/TiO_2 and CuO NPs(WI)/TNT, respectively (Fig. 24A(c)). The HER activity of this series of photocatalysts was measured in an aqueous solution containing methanol as a sacrificial agent. The results revealed that the HER activity of the photocatalysts increased in the following order: CuO NPs(A–C)/TNT > CuO NPs(WI)/TNT > CuO NPs(A–C)/TiO_2 > CuO NPs(WI)/TiO_2 (Fig. 24B). CuO NPs(A–C)/TNT showed the highest activity, which was higher than that of the corresponding photocatalyst using noble metal Pt/Ni NPs as a cocatalyst. Because TNTs are cylindrical, they have a high specific surface area (Fig. 24C). In addition, adsorption and

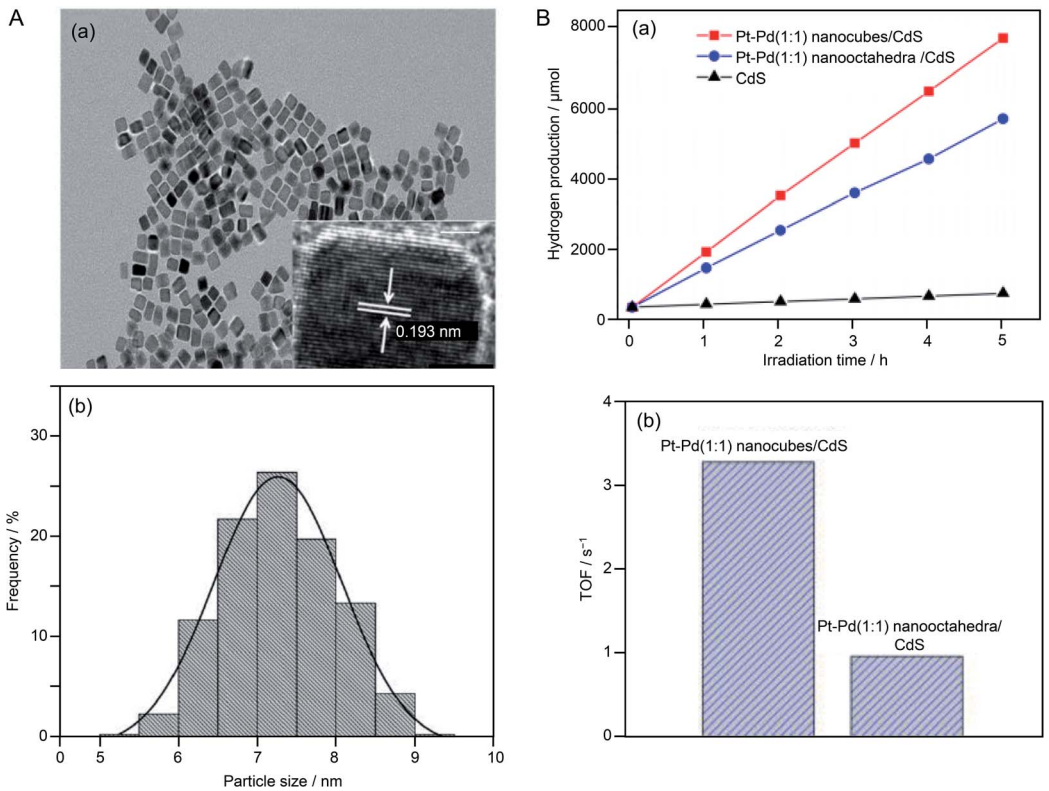

Fig. 23 (A) (a) TEM and high-resolution TEM images and (b) particle size distribution of Pt–Pd (1 : 1) alloy nanocubes (Pt–Pd (1 : 1) nanocubes). (B) (a) Irradiation time course for H_2 evolution over Pt–Pd (1 : 1) nanocubes/CdS, Pt–Pd (1 : 1) nano-octahedra/CdS, and bare CdS photocatalysts. (b) Photocatalytic turnover frequencies (TOF) of Pt–Pd nanocubes/CdS and Pt–Pd nano-octahedra/CdS photocatalysts. Reproduced with permission from ref. 218. Copyright 2016 American Chemical Society.

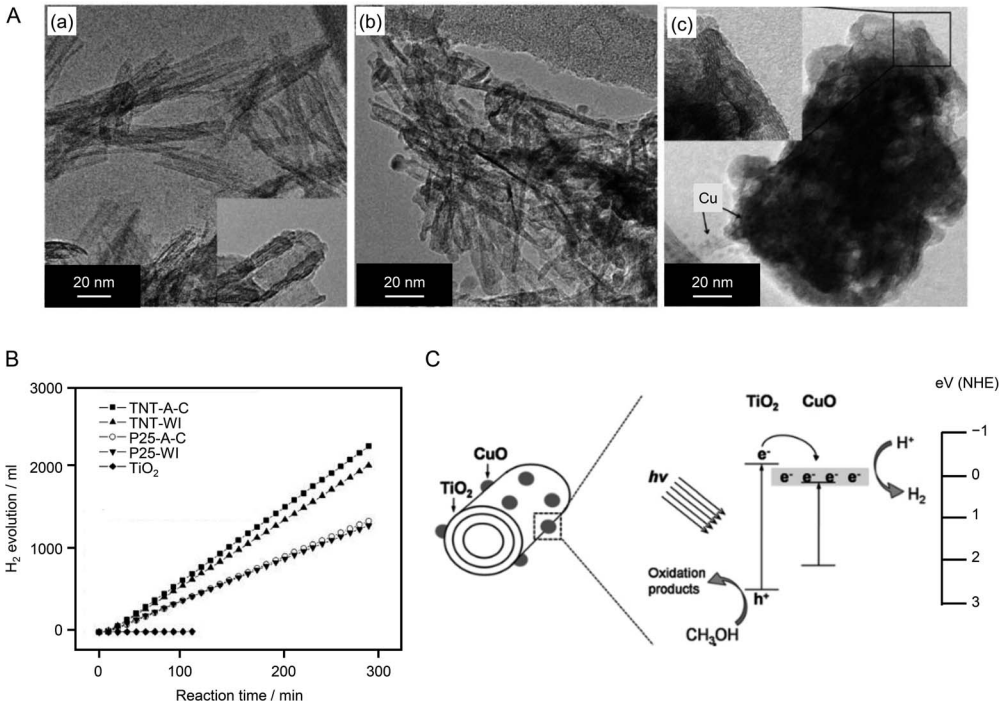

Fig. 24 (A) High-resolution TEM images of (a) TNT, (b) TNT-A–C, and (c) TNT-WI photocatalysts. (B) Time courses of H_2 evolution over the photocatalysts in (A) under irradiation. Inset: average H_2 evolution rates over 5 h of reaction. (C) Schematic diagram of charge transfer in the CuO NPs/TNT photocatalyst under irradiation. Reproduced with permission from ref. 219. Copyright 2011 Elsevier Ltd.

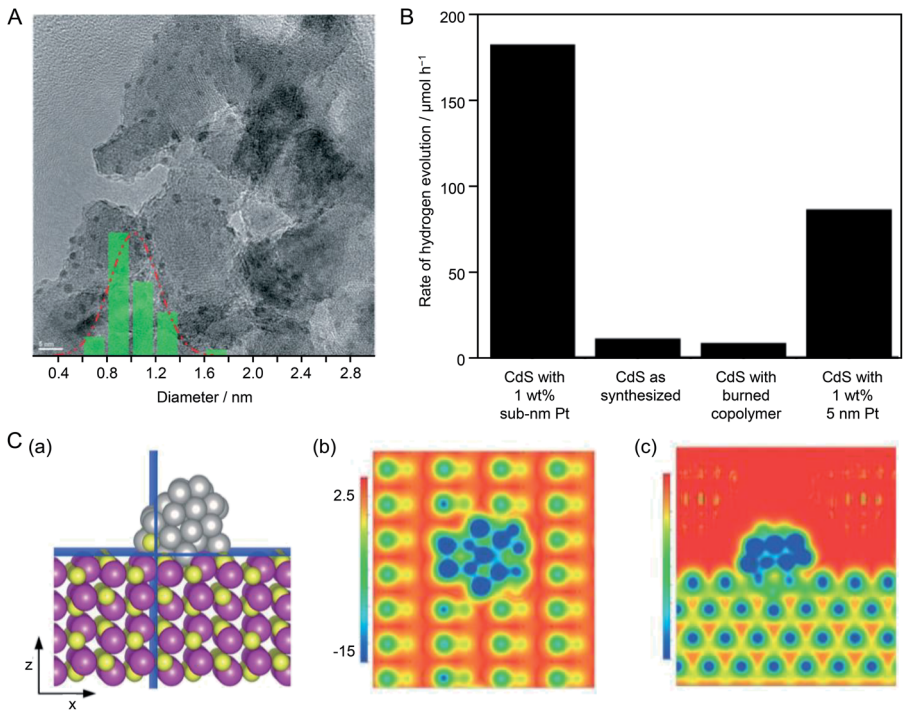

Fig. 25 (A) TEM image of 5 wt% Pt NCs loaded on Al_2O_3. The inset is the particle size distribution determined from the TEM image, showing an average Pt NC diameter of 0.9 ± 0.1 nm. (B) Rate of H_2 evolution of CdS under different conditions. (C) Contours of electrostatic surface potential of Pt_{38} NC/CdS on cutting planes that are normal to the (b) z-axis and (c) x-axis, as highlighted in blue in the structural model in (a). z- and x-axes are along the [1010] and [0001] directions, respectively. Potential energies are in eV. Reproduced with permission from ref. 220. Copyright 2015 The Royal Society of Chemistry.

calcination loaded cocatalyst NPs with higher dispersibility than that in the case of wet impregnation, and NP aggregation was less likely to occur in the former samples than in the latter. The high HER activity of CuO NPs(A–C)/TNT was ascribed to these factors.

4.2.2. Use of atomically precise colloidal metal NCs. In 2015, Orlov *et al.*[220] used metal NCs instead of metal NPs as HER cocatalysts. First, they synthesized fine PVP–Pt NCs by liquid-phase reduction. The obtained PVP–Pt NCs were adsorbed on CdS as a photocatalyst. Calcination of PVP–Pt NCs/CdS at 400 °C under reduced pressure for 24 h and then 400 °C under flowing hydrogen for 2 h gave Pt NCs/CdS. TEM measurements revealed that the loaded Pt NCs had an average particle size of only about 0.9 nm (Fig. 25A). The HER of the obtained Pt NCs/CdS photocatalyst was measured in an aqueous solution containing Na_2S and Na_2SO_3 as sacrificial agents. The HER activity of Pt NCs/CdS was 17 times higher than that of CdS without a cocatalyst (Fig. 25B). Also, Pt NCs/CdS showed higher HER activity than CdS with Pt NPs with a size of about 5 nm as a cocatalyst. These results indicated that Pt NCs are effective as HER cocatalysts and that miniaturization of cocatalysts can induce activation. Using a model in which a Pt_{38} NC was adsorbed on the CdS $(1\bar{0}10)$ plane, they investigated the interface structure and electronic interaction between the Pt NC and CdS in this composite system by a DFT calculation (Fig. 25C). The results revealed that the electronic structure and local surface potential changed on both the Pt NC and CdS surfaces because of the strong geometrical and electronic interactions between them. They stated that understanding the structural and electronic interactions between the NCs and photocatalyst is important for elucidating the reaction mechanism to optimize hydrogen production.

In the above study, although the cocatalyst (~0.9 nm) was in the size range of NCs, it is not clear whether the number of constituent atoms was controlled with atomic precision. In recent years, there have been several studies using NCs with atomic precision as cocatalyst precursors. In 2017, Yang *et al.*[221] studied the HER activity of photocatalyst systems using $[Ag_{25}(SPhMe_2)_{18}](PPh_4)$ ($SPhMe_2$ = 2,4-dimethylbenzenethiolate; PPh_4 = tetraphenylphosphine) and $[PtAg_{24}(SPhMe_2)_{18}](PPh_4)_2$ as cocatalyst precursors. $[Ag_{25}(SPhMe_2)_{18}](PPh_4)$ and $[PtAg_{24}(SPhMe_2)_{18}](PPh_4)_2$ were synthesized by the methods reported by Bakr *et al.*[222] and Zhu *et al.*,[223] respectively. Each type of NC was adsorbed on g-C_3N_4 by stirring for 12 h in a toluene/dichloromethane mixture with g-C_3N_4. The samples were calcined at 150 °C under flowing Ar for 2 h to yield Ag_{25} NC/g-C_3N_4 and $PtAg_{24}$ NC/g-C_3N_4. Both types of NCs had a particle size of about 1 nm. The removal of the ligands was confirmed by photoelectron spectroscopy. X-ray photoelectron spectroscopy and X-ray absorption fine structure analyses confirmed that Pt and Ag were in a zero-valent oxidation state in the NCs loaded on the photocatalyst. The photocatalysts were dispersed in an

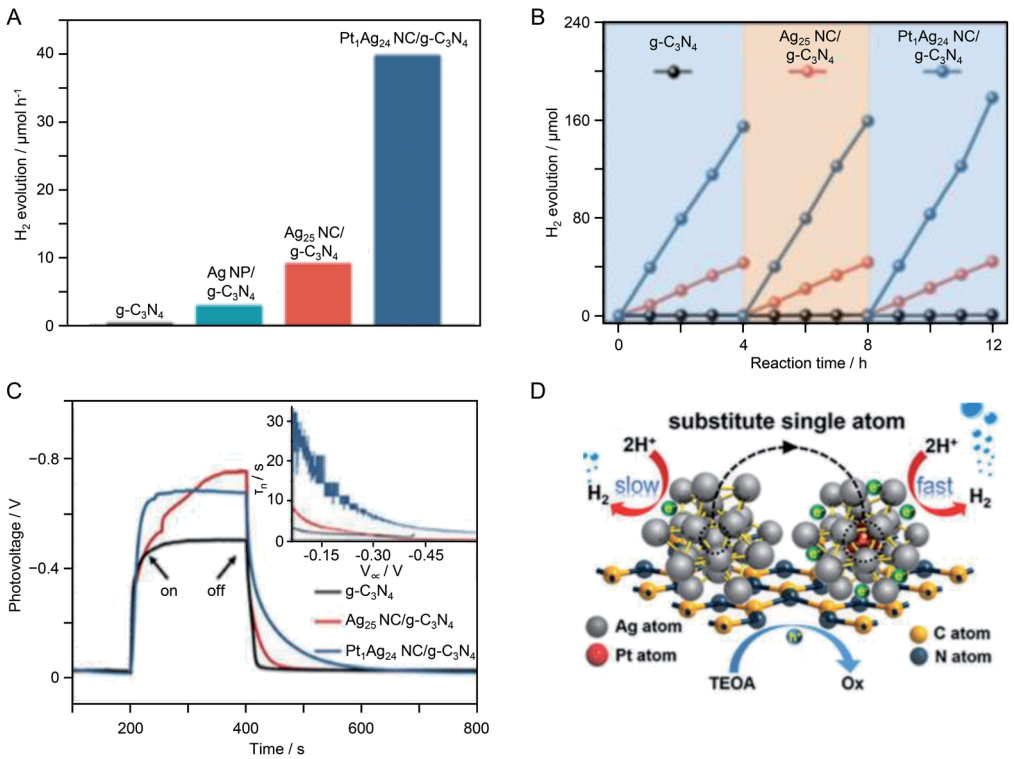

Fig. 26 Photocatalytic H_2 evolution performance. (A) Comparison of the photocatalytic H_2 evolution activities of g-C_3N_4, Ag NPs/g-C_3N_4, Ag_{25} NC/g-C_3N_4, and $PtAg_{24}$ NC/g-C_3N_4. (B) Cycling runs of photocatalytic H_2 evolution over g-C_3N_4, Ag_{25} NC/g-C_3N_4, and $PtAg_{24}$ NC/g-C_3N_4. (C) Transient OCVD measurements. The inset shows the average lifetimes of the photogenerated carriers (τ_n) obtained from the OCVD measurements. (D) Proposed photocatalytic H_2 evolution mechanism. Reproduced with permission from ref. 221. Copyright 2017 The Royal Society of Chemistry.

aqueous solution containing TEOA as a sacrificial agent and irradiated with visible light (>420 nm) to induce the HER. It was found that $PtAg_{24}$ NCs/g-C_3N_4 generated four times as much hydrogen as Ag_{25}/g-C_3N_4. The HER activity of $PtAg_{24}$ NC/g-C_3N_4 was 330 times higher than that of g-C_3N_4 without a cocatalyst (Fig. 26A and B). Open-circuit voltage decay (OCVD) measurements revealed that $PtAg_{24}$ NC/g-C_3N_4 had a longer carrier lifetime than that of Ag_{25} NC/g-C_3N_4 (Fig. 26C). The high HER activity of $PtAg_{24}$ NC/g-C_3N_4 was ascribed to effective trapping of the photoexcited electrons by Pt, which suppressed the recombination of electrons and holes (Fig. 26D). Thus, electron transfer was promoted by substituting one Ag atom of Ag_{25} with Pt, thereby improving the HER activity of the resulting NC-loaded photocatalyst.

In 2018, Fang *et al.*[224] also succeeded in improving the HER activity of g-C_3N_4 using precisely controlled metal NCs as a cocatalyst. They used $Au_{25}(Cys)_{18}$ with L-cysteine (Cys) as a ligand as a cocatalyst. First, $Au_{25}(Cys)_{18}$ (0.18, 0.49, or 0.96 wt%) and g-C_3N_4 were stirred in ethanol for 1 h to adsorb $Au_{25}(Cys)_{18}$ on g-C_3N_4. The obtained series of photocatalysts was dispersed in aqueous solutions containing TEOA as a sacrificial agent and then the HER was induced by irradiating the aqueous solution with visible light (>420 nm). The photocatalyst with 0.96 wt% $Au_{25}(Cys)_{18}$ exhibited the highest HER activity of the samples (Fig. 27A and B). Photoelectrochemical and photoluminescence measurements showed that the photocatalyst loaded with 0.96 wt% $Au_{25}(Cys)_{18}$ promoted charge separation to the greatest extent of the catalyst series. Based on these results, they concluded that the adsorption of $Au_{25}(Cys)_{18}$ not only provided HER active sites, but also induced effective interfacial charge transfer between the cocatalyst and g-C_3N_4 (Fig. 27C and D).

Thus, the precisely controlled NCs function as an effective HER cocatalysts. In addition, as described in Section 4.2, when precisely controlled NCs are used as a HER cocatalyst, it is easy to analyze the structure of the cocatalyst and clarify the origin of the improved activity. To utilize the advantages of such precise NCs, it is necessary to suppress aggregation of the cocatalyst on the photocatalyst surface. Section 4.2 revealed that the formation of a Cr_2O_3 shell suppressed both cocatalyst aggregation and the reverse reaction of water splitting. In 2019, Shi *et al.*[225] revealed that encapsulating precisely controlled NCs with metal–organic frameworks (MOFs) can also suppress the aggregation of NCs. In this study, Au_{25} was used as a precisely controlled NC and ZIF-8 was used as the MOF. First, $Au_{25}(SG)_{18}$ (~1.2 nm) was encapsulated into ZIF-8 by a coordination-assisted self-assembly strategy. Next, TiO_2 crystals were grown on the ZIF-8 surface by a hydrothermal method. Finally, a rhenium (Re) complex was adsorbed on the surface of the TiO_2 crystals to form ZIF-8/$Au_{25}(SG)_{18}$ NC/TiO_2-ReP with an Au content of 0.5 wt% (Fig. 28A). In this photocatalyst, $Au_{25}(SG)_{18}$ was used as an HER cocatalyst and the Re complex was used as a cocatalyst for the CO_2 reduction reaction. TEM measurements confirmed that during the preparation of ZIF-8/$Au_{25}(SG)_{18}$ NC/

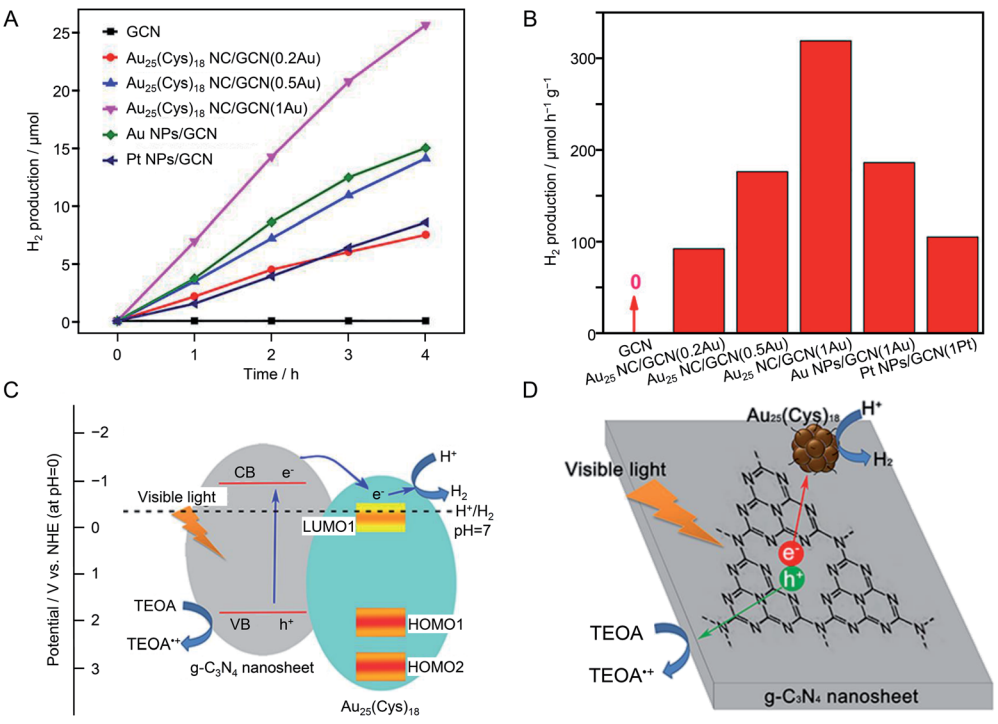

Fig. 27 (A) Plots of photocatalytic H_2 production under visible-light irradiation by g-C_3N_4 (GCN), $Au_{25}(Cys)_{18}$ NCs/GCN, Au NPs/GCN, and Pt NPs/GCN photocatalysts. (B) Rate of H_2 evolution by various $Au_{25}(Cys)_{18}$ NCs/GCN photocatalysts under visible light. (C) Energy diagram and (D) schematic diagram of photocatalytic H_2 evolution by $Au_{25}(Cys)_{18}$ NCs/GCN photocatalysts. Reproduced with permission from ref. 224. Copyright 2018 American Chemical Society.

TiO_2-ReP, the aggregation of $Au_{25}(SG)_{18}$ NC hardly occurred. The obtained photocatalyst was dispersed in an aqueous solution containing TEOA as a sacrificial agent and irradiated with visible light (>420 nm) to induce the HER and CO_2 reduction reaction. The HER activity of ZIF-8/$Au_{25}(SG)_{18}$ NC/TiO_2-ReP was about twice that of the case using Au NPs (~10 nm) as the HER cocatalyst. The turnover frequency of ZIF-8/$Au_{25}(SG)_{18}$ NC/TiO_2-ReP was 87 h^{-1} (based on an Au content of 0.5 wt%) and its apparent quantum yield at 500 nm was 2.06%. No decrease in activity was observed even when the light irradiation was continued for 7.5 h. In addition, high-angle annular dark field-STEM-energy-dispersive X-ray spectroscopy measurements indicated that the monodispersity of the $Au_{25}(SG)_{18}$ NC in ZIF-8/$Au_{25}(SG)_{18}$ NC/TiO_2-ReP was maintained after the photocatalytic reaction (Fig. 28B). These results demonstrated that encapsulating the cocatalyst with an MOF is also an effective way to produce stable and highly active photocatalysts.

4.2.3. Use of other controlled NPs/NCs. In this way, using the liquid-phase adsorption method makes it easy to control the particle size of the HER cocatalyst. On the other hand, there are several examples in which the particle size of the HER cocatalyst was successfully controlled by the conventional method. For example, in 2008, Mallouk *et al.* directly deposited $Rh(OH)_3$ NPs on the layers of Dion–Jacobson-type perovskite $HCa_2Nb_3O_{10}$ or $KCa_2Nb_3O_{10}$, and then calcinated the sample to uniformly load Rh_2O_3 NPs between the layers.[226] Fine Rh_2O_3 NPs were considered to be loaded in a highly dispersed state between the layers of $KCa_2Nb_3O_{10}$ because Rh^{3+} in $Rh(OH)_3$ NCs was immobilized

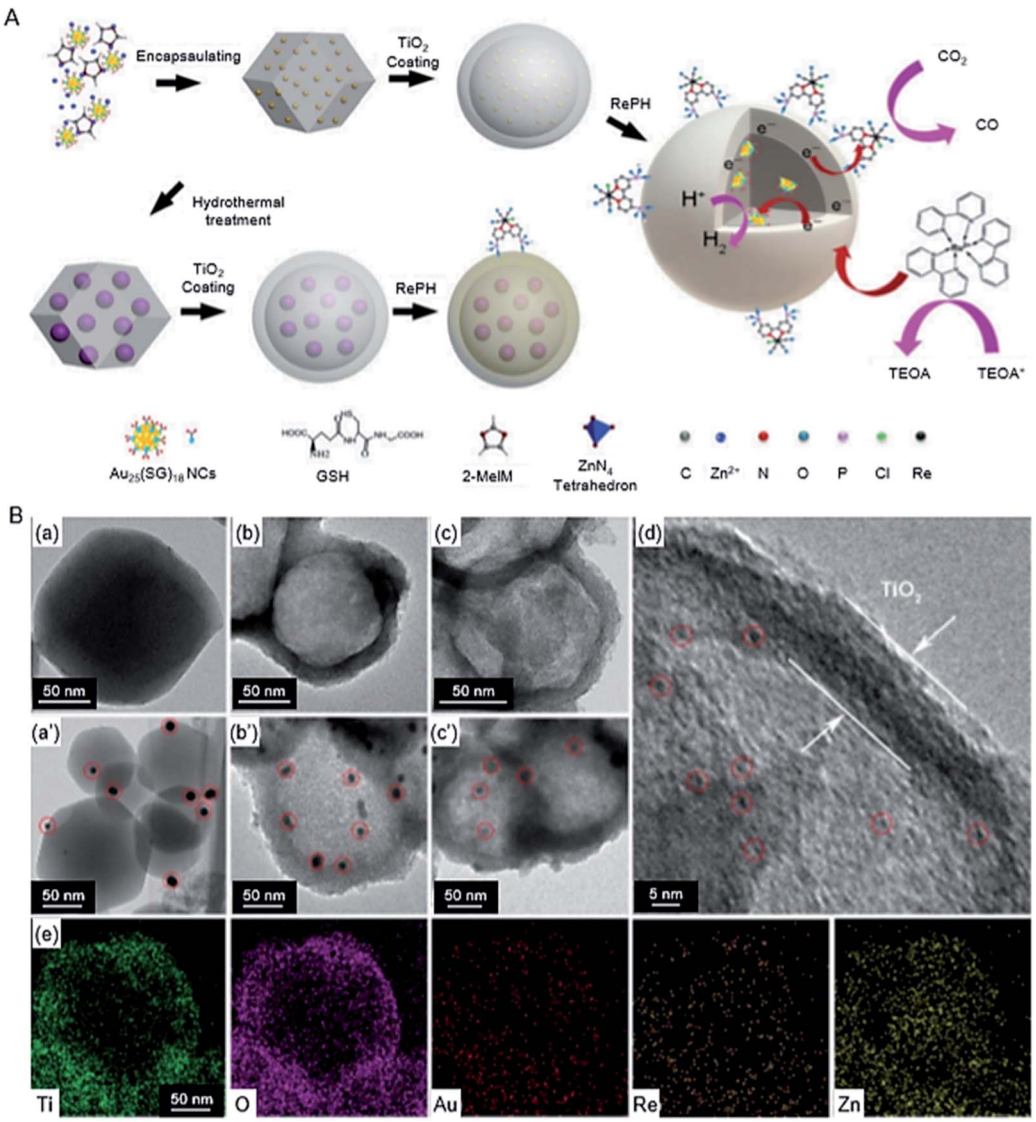

Fig. 28 (A) Fabrication of ZIF-8/$Au_{25}(SG)_{18}$ NC/TiO_2-ReP and ZIF-8/Au NPs/TiO_2-ReP composite photocatalysts by hydrothermal growth of a TiO_2 shell followed by grafting of RePH molecules, and the photocatalytic processes of CO_2 reduction and H_2 generation over ZIF-8/$Au_{25}(SG)_{18}$ NC/TiO_2-ReP under visible-light irradiation. (B) TEM images of (a) ZIF-8/$Au_{25}(SG)_{18}$ NC, (b) ZIF-8/$Au_{25}(SG)_{18}$ NC/TiO_2, (c) ZIF-8/$Au_{25}(SG)_{18}$ NC/TiO_2-ReP, (a′) ZIF-8/Au NPs, (b′) ZIF-8/Au NPs/TiO_2, and (c′) ZIF-8/Au NPs/TiO_2-ReP, and (d) high-resolution TEM image and (e) elemental maps of ZIF-8/$Au_{25}(SG)_{18}$ NC/TiO_2-ReP. Green: Ti, purple: O, red: Au, pink: Re, yellow: Zn. Reproduced with permission from ref. 225. Copyright 2019 Royal Society of Chemistry.

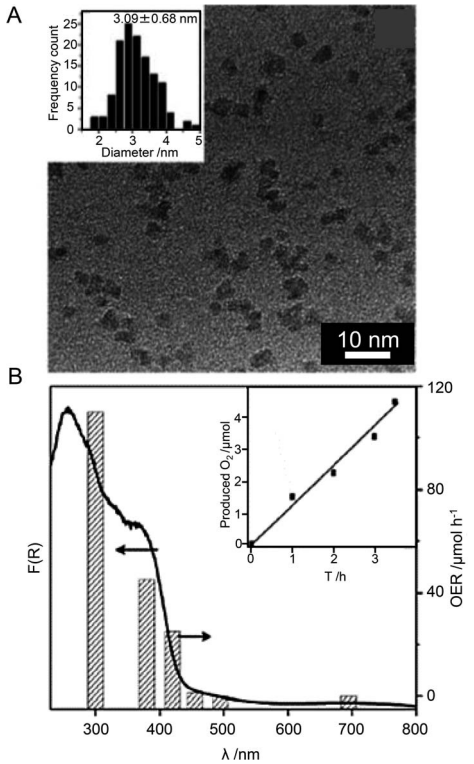

Fig. 29 (A) TEM image of as-prepared Co_3O_4 NPs. (B) Wavelength dependence O_2 evolution rate over 3 wt% Co_3O_4 NPs/g-C_3N_4. The inset is the O_2 evolution curves under visible light (λ > 455 nm). Reproduced with permission from ref. 227. Copyright 2017 Royal Society of Chemistry.

on the surface of the Nb oxide layer of the photocatalyst *via* covalent bonds (Rh–O–Nb) and thereby the formed Rh_2O_3 NPs couldn't aggregate on the surface of the Nb oxide layer. TEM images revealed that the loaded Rh_2O_3 NPs had a particle size of 0.7 ± 0.2 nm in the case of the loading amount of Rh being 1.0 wt%, whereas 1.1 ± 0.3 nm in the case of the loading amount of Rh being 10 wt%. Photocatalytic activity measurements revealed that the obtained Rh_2O_3 NPs/$KCa_2Nb_3O_{10}$ has high photocatalytic activity for H_2 evolution from aqueous methanol solution.

4.3. Application in O_2 evolution

4.3.1. Use of colloidal metal NPs. There are only a few examples of the use of metal NPs/NCs as OER photocatalysts. For example, in 2012, Wang *et al.* synthesized Co_3O_4 NPs by hydrothermal method and loaded them on g-C_3N_4.[227] TEM measurements confirmed that Co_3O_4 NPs with ~3 nm were loaded on g-C_3N_4 by this method. Such loading of Co_3O_4 NPs promoted the charge separation in the composite of Co_3O_4 NPs/g-C_3N_4 and showed an apparent quantum yield of 1.1% (at 420 nm) for oxygen production from aqueous silver nitrate solution (Fig. 29 and Table 3).

4.3.2. Use of other controlled NPs/NCs. Thus, there are only few examples of controlling the particle size of HER cocatalyst by liquid-phase adsorption method. On the other hand, there are some examples of controlling OER cocatalysts using the other method. For example, in 2017, Abe and colleagues have succeeded in controlling OER cocatalysts.[228] In this study, WO_3, $RuO_2 \cdot nH_2O$ NPs, and IO_3^-/I^- were used as the OER photocatalyst in a Z-scheme system (Fig. 4B), cocatalyst, and electron mediator, respectively. Because the reduction reaction of IO_3^- is a six-electron reaction, it is rate-limiting in the water-splitting reaction of Z-scheme systems. Therefore, it is necessary to load PtO_x or RuO_2 as a cocatalyst on the OER photocatalyst to accelerate this rate-limiting reaction. However, because the conventional loading method includes calcination, it is difficult to use this loading method for thermally unstable photocatalysts. Therefore, they attempted to load the cocatalyst on the photocatalyst ($RuO_2 \cdot nH_2O/WO_3$) simply by stirring the cocatalyst precursor ($RuCl_3$) and photocatalyst (WO_3) together in solution. They also prepared a sample that was calcined after adsorption for comparison (RuO_2/WO_3). These two photocatalysts were subjected to electrochemical measurements under light irradiation to evaluate their IO^{3-} reduction activity. $RuO_2 \cdot nH_2O/WO_3$ showed higher activity than RuO_2/WO_3 for the reduction of IO^{3-}. $RuO_2 \cdot nH_2O/WO_3$ also showed higher activity in the photocatalytic OER than RuO_2/WO_3. These results were attributed to $RuO_2 \cdot nH_2O$ loaded by just adsorption accelerating the IO_3^- reduction reaction more than RuO_2 loaded by a calcination process. Thus, the cocatalyst of the OER photocatalyst affects the reduction reaction rate of the electron mediator. This means that control of the cocatalyst of OER photocatalysts is also effective for enhancing the functionality of Z-scheme-type photocatalysts. This paper further showed that such a method is also effective for enhancing the activities of H_2WO_4 and Ta_3N_5, which are thermally unstable OER photocatalysts. In another recent paper, Maeda *et al.*[229] loaded RuO_2 on a nitrogen/fluorine-co-doped rutile TiO_2 (R–TiO_2:N,F) photocatalyst by the same loading method. This demonstrates that the adsorption method reported by Abe's group is highly versatile.

5. Information on interface between NPs/NCs and photocatalysts

In order to improve the functionality of water-splitting photocatalysts on the basis of the design guidelines, it is essential to

Table 3 Materials and experimental conditions in the study using liquid-phase adsorption method for oxygen production (half reaction)

	Cocatalyst					
Semiconductor	Kinds	Loading amount	Size	Light source	Reactant solution	Ref.
g-C_3N_4	Co_3O_4 NPs	3 wt%	~3 nm	300 W Xe lamp (λ > 455 nm)	0.01 M $AgNO_3$ aq.	227

elucidate the charge transfer rate, geometric and electronic structures, and interactions at the interface of NPs/NCs-photocatalysts. The measurements of the transient absorption and fluorescence decay are effective ways to determine the charge transfer rate.[230–235] For example, Lee *et al.* measured fluorescence decay of $Au_n(SG)_m$ NPs/ZnO and thereby elucidated that the rate of the charge transfer at the interface is enhanced as the size of the $Au_n(SG)_m$ increases.[235] For the elucidation of the geometrical/electronic structure of the loaded NPs/NCS and the surface of the substrate, scanning probing microscope (SPM) is a powerful tool.[236–238] For example, Diebold *et al.* successfully elucidated the growth pattern of Au NPs and Pt NCs on the surface (101) of anatase-type TiO_2 using the scanning tunneling microscope.[236] DFT calculations are promising for understanding the geometrical and electronic interaction at the interface.[239–243] For example, Libuda *et al.* performed DFT calculations on the model of Pt NPs/CeO_2 catalyst and found that there are two kinds of the strong interactions between Pt NPs and CeO_2, the electron transfer from Pt NPs to CeO_2 and the oxygen transfer from CeO_2 to Pt NPs. The latter effect was found to be unique to nanoscale CeO_2.[239]

Thus, spectroscopy, SPM, and DFT calculations are powerful tools for elucidating the phenomenon occurred at the interface of NPs/NCs-photocatalysis. In addition to these methods, electrochemical measurements are also useful for predicting the appropriate cocatalysts[121,122,244] because the overpotential obtained by electrochemical measurements are strongly related to the activation energy of each reaction. At present, these measurements and analyses have not been necessarily conducted for the photocatalysts described in Section 4. However, these measurements and analyses should be conducted also for the studies using the advanced water-splitting photocatalysts (Section 4). The results would provide a deeper understanding of their interfaces and enable us to predict the appropriate elements, size, and geometric structure of the cocatalysts suitable for obtaining highly active photocatalysts.

6. Summary

This review summarized recent studies on the application of metal NPs/NCs in water-splitting photocatalysis. Through this summary, the followings points regarding cocatalyst control were clarified.

(i) The use of precise synthesis and structure control techniques (nanotechnology) established in the fields of colloid, NP, and NC chemistry are effective for controlling the cocatalysts of water-splitting photocatalysts to obtain highly active water-splitting photocatalysts. At present, the kinds of ligands of the NPs/NCs and the photocatalysts used for liquid-phase adsorption method are limited to several species because this type of study just started in recent years. However, considering the mechanism (Section 3.2), other ligand-protected metal NPs/NCs[245] and photocatalysts[131] seem to be also applicable to the liquid-phase adsorption method.

(ii) To control a cocatalyst, it is very important to select appropriate elements, refine the particle size, improve dispersibility, form an alloy, form a shell with controlled thickness that suppresses the reverse reaction, expose a suitable crystal face, and control the charge state.

(iii) The formation of a shell that suppresses the reverse reaction is effective to enhance both the activity and stability of the cocatalyst.

(iv) Although the above-mentioned approaches provide an overall guidance to enhance cocatalyst activity, the most effective means to achieve high activation differs slightly depending on the combination of photocatalyst and cocatalyst.

(v) In one-step photoexcitation systems for overall water splitting, control of both HER and OER cocatalysts is effective for enhancing the overall activity of water-splitting photocatalysts.

(vi) For Z-scheme catalysts, reduction of the mediator may be rate-determining. Thus, control of the cocatalyst that promotes mediator reduction is an effective approach to increase the rate of this reaction.

(vii) Using precisely controlled NC cocatalysts provides a deeper understanding of geometrical structure and electronic state of the cocatalyst, and thereby greater knowledge of the main factors influencing photocatalyst activation.

These findings are expected to be useful for researchers in the field of water-splitting photocatalysis, as well as those interesting in the applications of controlled NPs/NCs.

7. Outlook

As mentioned above, it is necessary to improve the STH of a water-splitting photocatalyst to 10% or more to enable its practical use. Thus, the following studies are considered important in the future.

(i) Close collaboration between photocatalyst chemists and NP/NC chemists. To enhance the activity of water-splitting photocatalysts, it is necessary to improve both the semiconductor photocatalyst and cocatalyst. Regarding semiconductor photocatalysts, photocatalysis researchers would continue to make substantial improvements. On the other hand, the recent studies revealed that the use of precise synthesis and structure control techniques established in the fields of colloid, NP, and NC chemistry is very effective at raising cocatalyst activity. Therefore, researchers in the field of NPs/NCs should also conduct thorough research on enhancing the activity of cocatalysts. Effective approaches to maximize activation depend on the specific combination of photocatalyst and cocatalyst. If NCs/NPs researchers continue to conduct cocatalyst research using commercial photocatalysts, the results would not lead to the high activation of the most advanced photocatalysts. To develop highly active water-splitting photocatalysts for practical use, researchers in both fields need to collaborate more closely in future research.

(ii) Selective loading of cocatalysts on the optimal crystal plane. The crystal planes of semiconductor photocatalysts show different transport rates of photogenerated electrons and holes. If HER and OER cocatalysts could be selectively loaded on crystal planes with rapid electron and hole transport, electrons and holes could be efficiently used in the relevant reactions. In fact, research on photocatalysts in which a cocatalyst was

loaded by photodeposition demonstrated that such selective cocatalyst deposition is an effective approach to increase activation.[246] In the case of photodeposition, the HER cocatalyst is formed by reduction of metal ions and the OER cocatalyst is formed by oxidation of metal ions. Therefore, each cocatalyst is inevitably loaded on a crystal plane where electrons and holes can easily reach the active sites. Even for colloidal NPs/NCs, if such crystal plane-selective loading can be achieved, higher activity should be obtained compared with that provided by the present method. One of the methods seems to adsorb the colloidal metal NPs/NCs on the photocatalyst after a particular crystal-plane which is undesired site are selectively covered with a surfactant.

(iii) Control of the geometrical structure of loaded NPs/NCs. The geometrical structure of loaded NPs/NCs appears to show some variation. In the case of NPs, the size distribution occurs at the synthesis stage. In the case of NCs, there is no variation in size (chemical composition) and geometrical structure at the synthesis stage, but the NCs after loading sometimes seem to have varied geometrical structure. To identify the geometrical structures of NPs/NCs that lead to high activity and selectively load NPs/NCs with such geometrical structures as cocatalysts, it is necessary to establish a new method for controlling the geometrical structure of the loaded NPs/NCs. For NPs/NCs dispersed in solution, post-treatment methods for size[247] and structure convergence[55] have been reported. In the future, it is expected that post-treatment to achieve size and structure convergence will also be established for loaded NPs/NCs, which would realize the loading of NPs/NCs with controlled geometrical structure.

(iv) Elucidation of the calcination process. Protective organic molecules on colloidal metal NPs/NCs are often removed by calcination. However, the presence or absence of protective organic molecules is generally determined only by X-ray photoelectron spectroscopy and/or X-ray absorption fine structure measurements. In the case of NCs, although NCs are synthesized while controlling the chemical composition at the atomic/molecular level, ambiguity remains about the elimination of the protective ligands. For ultrafine NCs, the remaining protective ligands should strongly affect the electronic/geometrical structure of the NCs. To obtain reliable design guidelines for improving the activity of cocatalysts, it is necessary to determine whether or not the protective ligands remain on the NCs at the atomic/molecular level. Thus, it is necessary to gain a deep understanding of the calcination mechanism and to further improve the structural analysis techniques for loaded NCs. If the calcination mechanism can be clarified at the molecular level, it will not be necessary to consider the protective ligands remaining after calcination and will also be possible to conduct calcination at an appropriate temperature to suppress cocatalyst aggregation on the photocatalyst. This understanding is also necessary for better control of the geometrical structure of loaded NCs.

(v) Utilization of various metal NPs/NCs. In recent years, it has become possible to synthesize various monodisperse NPs/NCs with controlled size and structure. Inorganic chemists can now synthesize metal NCs as precisely as organic chemists synthesize organic molecules, and the types of synthesized NCs are steadily increasing. However, the types of NPs/NCs used in the study of water-splitting photocatalysts are limited. In the future, more of the existing NPs/NCs should be used in water-splitting photocatalysis research. This would expand knowledge of the major factors affecting cocatalyst activity and increase the possibility of producing photocatalysts with high water-splitting activity.

(vi) Theoretical calculations of real systems. For understanding the main factors influencing the activity, theoretical research using the actual geometrical structures is required. At present, deep understanding of the chemical composition and geometrical structure of loaded NPs/NCs and their loading sites on photocatalysts have not been obtained experimentally. In the future, it is expected that the structural analysis techniques for loaded NCs will be improved and thereby enable theoretical calculations to be carried out using actual geometrical structures obtained by such experiments. If such a progress would be achieved, it became possible to predict appropriate photocatalyst systems by DFT calculations.

We hope that by overcoming these current limitations of water-splitting photocatalysts, a society able to solve energy and environmental problems will emerge as soon as possible.

Authors contributions

Y. Negishi constructed the structure of this review. T. Kawawaki, Y. Mori, K. Wakamatsu, S. Ozaki, and M. Kawachi surveyed the literature, compiled figures and tables, and wrote the manuscript. Y. Negishi and S. Hossain revised the entire draft before submission. All authors have approved the final version of the manuscript.

Conflicts of interest

There are no conflicts to declare.

Acknowledgements

This work was supported by the Japan Society for the Promotion of Science (JSPS) KAKENHI (grant number JP16H04099, 16K21402, 20H02698, 20H02552), Scientific Research on Innovative Areas "Coordination Asymmetry" (grant number 17H05385 and 19H04595), and Scientific Research on Innovative Areas "Innovations for Light-Energy Conversion" (grant number 18H05178 and 20H05115). Funding from Asahi Glass Foundation, TEPCO Memorial Foundation Research Grant (Basic Research), and Kato Foundation for Promotion of Science (grant number KJ-2904) are also gratefully acknowledged.

References

1 C. N. R. Rao, P. J. Thomas and G. U. Kulkarni, *Nanocrystals: Synthesis, Properties and Applications*, Springer, Berlin Heidelberg, Germany, 2007.

2 B. Corain, G. Schmid and N. Toshima, *Metal Nanoclusters in Catalysis and Materials Science: The Issue of Size Control*, Elsevier B.V., Amsterdam, The Netherlands, 2008.
3 M. Faraday, *Philos. Trans. R. Soc. London*, 1857, **147**, 145–181.
4 C. M. Cobley, J. Chen, E. C. Cho, L. V. Wang and Y. Xia, *Chem. Soc. Rev.*, 2011, **40**, 44–56.
5 H.-L. Wu, R. Sato, A. Yamaguchi, M. Kimura, M. Haruta, H. Kurata and T. Teranishi, *Science*, 2016, **351**, 1306–1310.
6 T. Kawawaki, T. Nakagawa, M. Sakamoto and T. Teranishi, *J. Am. Chem. Soc.*, 2019, **141**, 8402–8406.
7 N. L. Rosi, D. A. Giljohann, C. S. Thaxton, A. K. R. Lytton-Jean, M. S. Han and C. A. Mirkin, *Science*, 2006, **312**, 1027–1030.
8 H. Zhang, T. Watanabe, M. Okumura, M. Haruta and N. Toshima, *Nat. Mater.*, 2012, **11**, 49–52.
9 B. Huang, H. Kobayashi, T. Yamamoto, S. Matsumura, Y. Nishida, K. Sato, K. Nagaoka, S. Kawaguchi, Y. Kubota and H. Kitagawa, *J. Am. Chem. Soc.*, 2017, **139**, 4643–4646.
10 T. Kawawaki, H. Wang, T. Kubo, K. Saito, J. Nakazaki, H. Segawa and T. Tatsuma, *ACS Nano*, 2015, **9**, 4165–4172.
11 T. Matsuura, K. Imaeda, S. Hasegawa, H. Suzuki and K. Imura, *J. Phys. Chem. Lett.*, 2019, **10**, 819–824.
12 N. J. Halas, S. Lal, W.-S. Chang, S. Link and P. Nordlander, *Chem. Rev.*, 2011, **111**, 3913–3961.
13 M. Sadakiyo, M. Kon-no, K. Sato, K. Nagaoka, H. Kasai, K. Kato and M. Yamauchi, *Dalton Trans.*, 2014, **43**, 11295–11298.
14 R. Takahata and T. Tsukuda, *Chem. Lett.*, 2019, **48**, 906–915.
15 T. Yonezawa, S. Onoue and N. Kimizuka, *Adv. Mater.*, 2001, **13**, 140–142.
16 M. Basu, A. K. Sinha, M. Pradhan, S. Sarkar, Y. Negishi, Govind and T. Pal, *Environ. Sci. Technol.*, 2010, **44**, 6313–6318.
17 F. Mafuné, J.-y. Kohno, Y. Takeda, T. Kondow and H. Sawabe, *J. Phys. Chem. B*, 2000, **104**, 9111–9117.
18 H. Kawasaki, *Nanotechnol. Rev.*, 2013, **2**, 5–25.
19 Y.-w. Jun, J.-H. Lee and J. Cheon, *Angew. Chem., Int. Ed.*, 2008, **47**, 5122–5135.
20 K. G. Thomas and P. V. Kamat, *J. Am. Chem. Soc.*, 2000, **122**, 2655–2656.
21 T. Suzuki, K.-i. Okazaki, S. Suzuki, T. Shibayama, S. Kuwabata and T. Torimoto, *Chem. Mater.*, 2010, **22**, 5209–5215.
22 M. Miyachi, Y. Yamanoi, Y. Shibata, H. Matsumoto, K. Nakazato, M. Konno, K. Ito, Y. Inoue and H. Nishihara, *Chem. Commun.*, 2010, **46**, 2557–2559.
23 T. Oshikiri, K. Ueno and H. Misawa, *Angew. Chem., Int. Ed.*, 2016, **55**, 3942–3946.
24 K. L. Kelly, E. Coronado, L. L. Zhao and G. C. Schatz, *J. Phys. Chem. B*, 2003, **107**, 668–677.
25 Y. Tian and T. Tatsuma, *J. Am. Chem. Soc.*, 2005, **127**, 7632–7637.
26 Y. Takahashi, Y. Sota, T. Ishida, Y. Furukawa and S. Yamada, *J. Phys. Chem. C*, 2020, **124**, 4202–4205.
27 R. B. M. Schasfoort, *Handbook of Surface Plasmon Resonance*, Royal Society of Chemistry, Cambridge, 2017.
28 S.-Y. Ding, J. Yi, J.-F. Li, B. Ren, D.-Y. Wu, R. Panneerselvam and Z.-Q. Tian, *Nat. Rev. Mater.*, 2016, **1**, 16021.
29 F. Toderas, M. Baia, L. Baia and S. Astilean, *Nanotechnology*, 2007, **18**, 255702.
30 B.-H. Sohn, J.-M. Choi, S. I. Yoo, S.-H. Yun, W.-C. Zin, J. C. Jung, M. Kanehara, T. Hirata and T. Teranishi, *J. Am. Chem. Soc.*, 2003, **125**, 6368–6369.
31 R. Singh and J. W. Lillard, *Exp. Mol. Pathol.*, 2009, **86**, 215–223.
32 S. M. Lang and T. M. Bernhardt, *Phys. Chem. Chem. Phys.*, 2012, **14**, 9255–9269.
33 T. Tsukuda and H. Häkkinen, *Protected Metal Clusters: From Fundamentals to Applications*, Elsevier B.V., Amsterdam, The Netherlands, 2015.
34 R. Jin, C. Zeng, M. Zhou and Y. Chen, *Chem. Rev.*, 2016, **116**, 10346–10413.
35 R. Jin, *Nanoscale*, 2010, **2**, 343–362.
36 R. R. Nasaruddin, T. Chen, N. Yan and J. Xie, *Coord. Chem. Rev.*, 2018, **368**, 60–79.
37 Y. Du, H. Sheng, D. Astruc and M. Zhu, *Chem. Rev.*, 2020, **120**, 526–622.
38 N. A. Sakthivel and A. Dass, *Acc. Chem. Res.*, 2018, **51**, 1774–1783.
39 H. Kawasaki, S. Kumar, G. Li, C. Zeng, D. R. Kauffman, J. Yoshimoto, Y. Iwasaki and R. Jin, *Chem. Mater.*, 2014, **26**, 2777–2788.
40 K. Yamamoto, T. Imaoka, M. Tanabe and T. Kambe, *Chem. Rev.*, 2020, **120**, 1397–1437.
41 R. L. Whetten, H.-C. Weissker, J. J. Pelayo, S. M. Mullins, X. López-Lozano and I. L. Garzón, *Acc. Chem. Res.*, 2019, **52**, 34–43.
42 S. Sharma, K. K. Chakrahari, J.-Y. Saillard and C. W. Liu, *Acc. Chem. Res.*, 2018, **51**, 2475–2483.
43 M.-L. Cui, Y.-S. Chen, Q.-F. Xie, D.-P. Yang and M.-Y. Han, *Coord. Chem. Rev.*, 2019, **387**, 450–462.
44 J. Fang, B. Zhang, Q. Yao, Y. Yang, J. Xie and N. Yan, *Coord. Chem. Rev.*, 2016, **322**, 1–29.
45 T.-Q. Yang, B. Peng, B.-Q. Shan, Y.-X. Zong, J.-G. Jiang, P. Wu and K. Zhang, *Nanomaterials*, 2020, **10**, 261.
46 Y. Negishi, W. Kurashige, Y. Niihori, T. Iwasa and K. Nobusada, *Phys. Chem. Chem. Phys.*, 2010, **12**, 6219–6225.
47 Y. Negishi, T. Iwai and M. Ide, *Chem. Commun.*, 2010, **46**, 4713–4715.
48 Y. Negishi, W. Kurashige, Y. Kobayashi, S. Yamazoe, N. Kojima, M. Seto and T. Tsukuda, *J. Phys. Chem. Lett.*, 2013, **4**, 3579–3583.
49 Y. Negishi, K. Munakata, W. Ohgake and K. Nobusada, *J. Phys. Chem. Lett.*, 2012, **3**, 2209–2214.
50 Y. Niihori, M. Matsuzaki, T. Pradeep and Y. Negishi, *J. Am. Chem. Soc.*, 2013, **135**, 4946–4949.
51 Y. Niihori, M. Matsuzaki, C. Uchida and Y. Negishi, *Nanoscale*, 2014, **6**, 7889–7896.
52 Y. Niihori, Y. Kikuchi, A. Kato, M. Matsuzaki and Y. Negishi, *ACS Nano*, 2015, **9**, 9347–9356.
53 Y. Niihori, M. Eguro, A. Kato, S. Sharma, B. Kumar, W. Kurashige, K. Nobusada and Y. Negishi, *J. Phys. Chem. C*, 2016, **120**, 14301–14309.

54 Y. Niihori, Y. Koyama, S. Watanabe, S. Hashimoto, S. Hossain, L. V. Nair, B. Kumar, W. Kurashige and Y. Negishi, *J. Phys. Chem. Lett.*, 2018, **9**, 4930–4934.
55 Y. Niihori, S. Hashimoto, Y. Koyama, S. Hossain, W. Kurashige and Y. Negishi, *J. Phys. Chem. C*, 2019, **123**, 13324–13329.
56 Y. Niihori, D. Shima, K. Yoshida, K. Hamada, L. V. Nair, S. Hossain, W. Kurashige and Y. Negishi, *Nanoscale*, 2018, **10**, 1641–1649.
57 T. G. Dietz, M. A. Duncan, D. E. Powers and R. E. Smalley, *J. Chem. Phys.*, 1981, **74**, 6511–6512.
58 R. E. Leuchtner, A. C. Harms and A. W. Castleman Jr, *J. Chem. Phys.*, 1989, **91**, 2753–2754.
59 G. Ganteför, K. H. Meiwes-Broer and H. O. Lutz, *Phys. Rev. A: At., Mol., Opt. Phys.*, 1988, **37**, 2716–2718.
60 J. R. R. Verlet, A. E. Bragg, A. Kammrath, O. Cheshnovsky and D. M. Neumark, *J. Chem. Phys.*, 2004, **121**, 10015–10025.
61 K. Miyajima, N. Fukushima, H. Himeno, A. Yamada and F. Mafuné, *J. Phys. Chem. A*, 2009, **113**, 13448–13450.
62 A. Nakajima, K. Hoshino, K. Watanabe, Y. Konishi, T. Kurikawa, S. Iwata and K. Kaya, *Chem. Phys. Lett.*, 1994, **222**, 353–357.
63 Y. Negishi, Y. Nakamura, A. Nakajima and K. Kaya, *J. Chem. Phys.*, 2001, **115**, 3657–3663.
64 K. Tono, A. Terasaki, T. Ohta and T. Kondow, *Chem. Phys. Lett.*, 2007, **449**, 276–281.
65 T. Watanabe and T. Tsukuda, *J. Phys. Chem. C*, 2013, **117**, 6664–6668.
66 A. von Weber and S. L. Anderson, *Acc. Chem. Res.*, 2016, **49**, 2632–2639.
67 Y. Negishi, H. Kawamata, A. Nakajima and K. Kaya, *J. Electron Spectrosc. Relat. Phenom.*, 2000, **106**, 117–125.
68 J. Li, X. Li, H.-J. Zhai and L.-S. Wang, *Science*, 2003, **299**, 864–867.
69 K. Judai, S. Abbet, A. S. Wörz, U. Heiz and C. R. Henry, *J. Am. Chem. Soc.*, 2004, **126**, 2732–2737.
70 C. E. Briant, B. R. C. Theobald, J. W. White, L. K. Bell, D. M. P. Mingos and A. J. Welch, *J. Chem. Soc., Chem. Commun.*, 1981, 201–202.
71 G. Schmid, R. Pfeil, R. Boese, F. Bandermann, S. Meyer, G. H. M. Calis and J. W. A. van der Velden, *Chem. Ber.*, 1981, **114**, 3634–3642.
72 S. S. Kurasov, N. K. Eremenko, Y. L. Slovokhotov and Y. T. Struchkov, *J. Organomet. Chem.*, 1989, **361**, 405–408.
73 M. McPartlin, R. Mason and L. Malatesta, *J. Chem. Soc. D*, 1969, 334.
74 E. G. Mednikov and L. F. Dahl, *Philos. Trans. R. Soc., A*, 2010, **368**, 1301–1332.
75 G. Schmid, *Chem. Rev.*, 1992, **92**, 1709–1727.
76 M. Schulz-Dobrick and M. Jansen, *Z. Anorg. Allg. Chem.*, 2007, **633**, 2326–2331.
77 B. K. Teo, X. Shi and H. Zhang, *J. Am. Chem. Soc.*, 1992, **114**, 2743–2745.
78 F. A. Vollenbroek, J. J. Bour and J. W. A. van der Veden, *Recl. Trav. Chim. Pays-Bas*, 1980, **99**, 137–141.
79 I. Chakraborty and T. Pradeep, *Chem. Rev.*, 2017, **117**, 8208–8271.
80 M. Brust, M. Walker, D. Bethell, D. J. Schiffrin and R. Whyman, *J. Chem. Soc., Chem. Commun.*, 1994, 801–802.
81 Y. Negishi, K. Nobusada and T. Tsukuda, *J. Am. Chem. Soc.*, 2005, **127**, 5261–5270.
82 M. Agrachev, M. Ruzzi, A. Venzo and F. Maran, *Acc. Chem. Res.*, 2019, **52**, 44–52.
83 B. Bhattarai, Y. Zaker, A. Atnagulov, B. Yoon, U. Landman and T. P. Bigioni, *Acc. Chem. Res.*, 2018, **51**, 3104–3113.
84 Z. Gan, N. Xia and Z. Wu, *Acc. Chem. Res.*, 2018, **51**, 2774–2783.
85 A. Ghosh, O. F. Mohammed and O. M. Bakr, *Acc. Chem. Res.*, 2018, **51**, 3094–3103.
86 S. Hossain, Y. Niihori, L. V. Nair, B. Kumar, W. Kurashige and Y. Negishi, *Acc. Chem. Res.*, 2018, **51**, 3114–3124.
87 K. Kwak and D. Lee, *Acc. Chem. Res.*, 2019, **52**, 12–22.
88 B. Nieto-Ortega and T. Bürgi, *Acc. Chem. Res.*, 2018, **51**, 2811–2819.
89 J. Yan, B. K. Teo and N. Zheng, *Acc. Chem. Res.*, 2018, **51**, 3084–3093.
90 Q. Yao, T. Chen, X. Yuan and J. Xie, *Acc. Chem. Res.*, 2018, **51**, 1338–1348.
91 M. A. Bakar, M. Sugiuchi, M. Iwasaki, Y. Shichibu and K. Konishi, *Nat. Commun.*, 2017, **8**, 576.
92 Q.-F. Zhang, X. Chen and L.-S. Wang, *Acc. Chem. Res.*, 2018, **51**, 2159–2168.
93 Z. Lei, X.-K. Wan, S.-F. Yuan, Z.-J. Guan and Q.-M. Wang, *Acc. Chem. Res.*, 2018, **51**, 2465–2474.
94 S. Takano, S. Hasegawa, M. Suyama and T. Tsukuda, *Acc. Chem. Res.*, 2018, **51**, 3074–3083.
95 Y. Niihori, W. Kurashige, M. Matsuzaki and Y. Negishi, *Nanoscale*, 2013, **5**, 508–512.
96 S. Xie, H. Tsunoyama, W. Kurashige, Y. Negishi and T. Tsukuda, *ACS Catal.*, 2012, **2**, 1519–1523.
97 Y. Negishi, K. Igarashi, K. Munakata, W. Ohgake and K. Nobusada, *Chem. Commun.*, 2012, **48**, 660–662.
98 S. Yamazoe, W. Kurashige, K. Nobusada, Y. Negishi and T. Tsukuda, *J. Phys. Chem. C*, 2014, **118**, 25284–25290.
99 S. Hossain, T. Ono, M. Yoshioka, G. Hu, M. Hosoi, Z. Chen, L. V. Nair, Y. Niihori, W. Kurashige, D.-e. Jiang and Y. Negishi, *J. Phys. Chem. Lett.*, 2018, **9**, 2590–2594.
100 S. Sharma, W. Kurashige, K. Nobusada and Y. Negishi, *Nanoscale*, 2015, **7**, 10606–10612.
101 S. Sharma, S. Yamazoe, T. Ono, W. Kurashige, Y. Niihori, K. Nobusada, T. Tsukuda and Y. Negishi, *Dalton Trans.*, 2016, **45**, 18064–18068.
102 L. V. Nair, S. Hossain, S. Takagi, Y. Imai, G. Hu, S. Wakayama, B. Kumar, W. Kurashige, D.-e. Jiang and Y. Negishi, *Nanoscale*, 2018, **10**, 18969–18979.
103 W. Kurashige, M. Yamaguchi, K. Nobusada and Y. Negishi, *J. Phys. Chem. Lett.*, 2012, **3**, 2649–2652.
104 W. Kurashige, K. Munakata, K. Nobusada and Y. Negishi, *Chem. Commun.*, 2013, **49**, 5447–5449.
105 S. Hossain, Y. Imai and Y. Negishi, *AIP Conf. Proc.*, 2019, **2186**, 030018.
106 S. Hossain, Y. Imai, Y. Motohashi, Z. Chen, D. Suzuki, T. Suzuki, Y. Kataoka, M. Hirata, T. Ono, W. Kurashige,

T. Kawawaki, T. Yamamoto and Y. Negishi, *Mater. Horiz.*, 2020, **7**, 796–803.
107 S. Hossain, Y. Imai, D. Suzuki, W. Choi, Z. Chen, T. Suzuki, M. Yoshioka, T. Kawawaki, D. Lee and Y. Negishi, *Nanoscale*, 2019, **11**, 22089–22098.
108 Y. Shichibu, Y. Negishi, T. Watanabe, N. K. Chaki, H. Kawaguchi and T. Tsukuda, *J. Phys. Chem. C*, 2007, **111**, 7845–7847.
109 N. Barrabés, B. Zhang and T. Bürgi, *J. Am. Chem. Soc.*, 2014, **136**, 14361–14364.
110 P. D. Jadzinsky, G. Calero, C. J. Ackerson, D. A. Bushnell and R. D. Kornberg, *Science*, 2007, **318**, 430–433.
111 M. W. Heaven, A. Dass, P. S. White, K. M. Holt and R. W. Murray, *J. Am. Chem. Soc.*, 2008, **130**, 3754–3755.
112 M. Zhu, C. M. Aikens, F. J. Hollander, G. C. Schatz and R. Jin, *J. Am. Chem. Soc.*, 2008, **130**, 5883–5885.
113 H. Qian, W. T. Eckenhoff, Y. Zhu, T. Pintauer and R. Jin, *J. Am. Chem. Soc.*, 2010, **132**, 8280–8281.
114 Y. Chen, C. Zeng, C. Liu, K. Kirschbaum, C. Gayathri, R. R. Gil, N. L. Rosi and R. Jin, *J. Am. Chem. Soc.*, 2015, **137**, 10076–10079.
115 T. Kawawaki, Y. Negishi and H. Kawasaki, *Nanoscale Adv.*, 2020, **2**, 17–36.
116 T. Kawawaki and Y. Negishi, *Nanomaterials*, 2020, **10**, 238.
117 A. Munir, K. S. Joya, T. Ul haq, N.-U.-A. Babar, S. Z. Hussain, A. Qurashi, N. Ullah and I. Hussain, *ChemSusChem*, 2019, **12**, 1517–1548.
118 R. Shi, Y. Cao, Y. Bao, Y. Zhao, G. I. N. Waterhouse, Z. Fang, L.-Z. Wu, C.-H. Tung, Y. Yin and T. Zhang, *Adv. Mater.*, 2017, **29**, 1700803.
119 L. Shang, Y. Liang, M. Li, G. I. N. Waterhouse, P. Tang, D. Ma, L.-Z. Wu, C.-H. Tung and T. Zhang, *Adv. Funct. Mater.*, 2017, **27**, 1606215.
120 Y. Cao, J. Guo, R. Shi, G. I. N. Waterhouse, J. Pan, Z. Du, Q. Yao, L.-Z. Wu, C.-H. Tung, J. Xie and T. Zhang, *Nat. Commun.*, 2018, **9**, 2379.
121 J. Lu, Z. Tang, L. Luo, S. Yin, P. Kang Shen and P. Tsiakaras, *Appl. Catal., B*, 2019, **255**, 117737.
122 L. Zhang, J. Lu, S. Yin, L. Luo, S. Jing, A. Brouzgou, J. Chen, P. K. Shen and P. Tsiakaras, *Appl. Catal., B*, 2018, **230**, 58–64.
123 A. Fujishima and K. Honda, *Nature*, 1972, **238**, 37–38.
124 K. Maeda and K. Domen, *J. Phys. Chem. Lett.*, 2010, **1**, 2655–2661.
125 X.-T. Wang, T. Ouyang, L. Wang, J.-H. Zhong and Z.-Q. Liu, *Angew. Chem., Int. Ed.*, 2020, **59**, 6492–6499.
126 C. Huang, Y. Zou, Y.-Q. Ye, T. Ouyang, K. Xiao and Z.-Q. Liu, *Chem. Commun.*, 2019, **55**, 7687–7690.
127 M. K. Sheehan, M. Rudden, H. Cai and C.-K. Tsung, *Catal. Lett.*, 2016, **146**, 309–318.
128 L. Liu, X. Zhang, L. Yang, L. Ren, D. Wang and J. Ye, *Natl. Sci. Rev.*, 2017, **4**, 761–780.
129 C. Jiang, S. J. A. Moniz, A. Wang, T. Zhang and J. Tang, *Chem. Soc. Rev.*, 2017, **46**, 4645–4660.
130 M. G. Walter, E. L. Warren, J. R. McKone, S. W. Boettcher, Q. Mi, E. A. Santori and N. S. Lewis, *Chem. Rev.*, 2010, **110**, 6446–6473.
131 A. Kudo and Y. Miseki, *Chem. Soc. Rev.*, 2009, **38**, 253–278.
132 K. Maeda, *ACS Catal.*, 2013, **3**, 1486–1503.
133 J. Yang, D. Wang, H. Han and C. Li, *Acc. Chem. Res.*, 2013, **46**, 1900–1909.
134 W. Kurashige, Y. Niihori, S. Sharma and Y. Negishi, *Coord. Chem. Rev.*, 2016, **320–321**, 238–250.
135 Y. Negishi, *Bull. Chem. Soc. Jpn.*, 2014, **87**, 375–389.
136 W. Kurashige, R. Kumazawa, S. Yoshino and Y. Negishi, in *Encyclopedia of Interfacial Chemistry*, ed. K. Wandelt, Elsevier, Oxford, 2018, pp. 683–696.
137 H. N. Kagalwala, E. Gottlieb, G. Li, T. Li, R. Jin and S. Bernhard, *Inorg. Chem.*, 2013, **52**, 9094–9101.
138 Y.-S. Chen and P. V. Kamat, *J. Am. Chem. Soc.*, 2014, **136**, 6075–6082.
139 Z. Luo, X. Yuan, Y. Yu, Q. Zhang, D. T. Leong, J. Y. Lee and J. Xie, *J. Am. Chem. Soc.*, 2012, **134**, 16662–16670.
140 H. Wang, F. Chen, W. Li and T. Tian, *J. Power Sources*, 2015, **287**, 150–157.
141 F.-X. Xiao and B. Liu, *Nanoscale*, 2017, **9**, 17118–17132.
142 K. Sridharan, E. Jang, J. H. Park, J.-H. Kim, J.-H. Lee and T. J. Park, *Chem.–Eur. J.*, 2015, **21**, 9126–9132.
143 H. Yang, L. Shang, Q. Zhang, R. Shi, G. I. N. Waterhouse, L. Gu and T. Zhang, *Nat. Commun.*, 2019, **10**, 4585.
144 M.-Z. Ge, C.-Y. Cao, S.-H. Li, Y.-X. Tang, L.-N. Wang, N. Qi, J.-Y. Huang, K.-Q. Zhang, S. S. Al-Deyab and Y.-K. Lai, *Nanoscale*, 2016, **8**, 5226–5234.
145 Y. Miseki, H. Kato and A. Kudo, *Energy Environ. Sci.*, 2009, **2**, 306–314.
146 Q. Wang and K. Domen, *Chem. Rev.*, 2020, **120**, 919–985.
147 Y. Wang, H. Suzuki, J. Xie, O. Tomita, D. J. Martin, M. Higashi, D. Kong, R. Abe and J. Tang, *Chem. Rev.*, 2018, **118**, 5201–5241.
148 G. Zhang, Z.-A. Lan, L. Lin, S. Lin and X. Wang, *Chem. Sci.*, 2016, **7**, 3062–3066.
149 X. Li, J. Yu, J. Low, Y. Fang, J. Xiao and X. Chen, *J. Mater. Chem. A*, 2015, **3**, 2485–2534.
150 T. Hisatomi, J. Kubota and K. Domen, *Chem. Soc. Rev.*, 2014, **43**, 7520–7535.
151 Z. Wang, C. Li and K. Domen, *Chem. Soc. Rev.*, 2019, **48**, 2109–2125.
152 X. Chen, S. Shen, L. Guo and S. S. Mao, *Chem. Rev.*, 2010, **110**, 6503–6570.
153 K. Domen, S. Naito, M. Soma, T. Onishi and K. Tamaru, *J. Chem. Soc., Chem. Commun.*, 1980, 543–544.
154 S. Sato and J. M. White, *Chem. Phys. Lett.*, 1980, **72**, 83–86.
155 J. M. Lehn, J. P. Sauvage and R. Ziessel, *Nouv. J. Chim.*, 1980, **4**, 623–627.
156 W.-J. Ong, L.-L. Tan, Y. H. Ng, S.-T. Yong and S.-P. Chai, *Chem. Rev.*, 2016, **116**, 7159–7329.
157 J. Liu, Y. Liu, N. Liu, Y. Han, X. Zhang, H. Huang, Y. Lifshitz, S.-T. Lee, J. Zhong and Z. Kang, *Science*, 2015, **347**, 970–974.
158 H. Kato, M. Hori, R. Konta, Y. Shimodaira and A. Kudo, *Chem. Lett.*, 2004, **33**, 1348–1349.
159 R. Konta, T. Ishii, H. Kato and A. Kudo, *J. Phys. Chem. B*, 2004, **108**, 8992–8995.
160 K. Maeda and K. Domen, *Chem. Mater.*, 2010, **22**, 612–623.

161 I. Tsuji, H. Kato and A. Kudo, *Angew. Chem., Int. Ed.*, 2005, **44**, 3565–3568.
162 T. Hisatomi, S. Okamura, J. Liu, Y. Shinohara, K. Ueda, T. Higashi, M. Katayama, T. Minegishi and K. Domen, *Energy Environ. Sci.*, 2015, **8**, 3354–3362.
163 M. G. Kibria, F. A. Chowdhury, S. Zhao, B. AlOtaibi, M. L. Trudeau, H. Guo and Z. Mi, *Nat. Commun.*, 2015, **6**, 6797.
164 S. Sun, T. Hisatomi, Q. Wang, S. Chen, G. Ma, J. Liu, S. Nandy, T. Minegishi, M. Katayama and K. Domen, *ACS Catal.*, 2018, **8**, 1690–1696.
165 A. Kudo, K. Ueda, H. Kato and I. Mikami, *Catal. Lett.*, 1998, **53**, 229–230.
166 A. Kudo, K. Omori and H. Kato, *J. Am. Chem. Soc.*, 1999, **121**, 11459–11467.
167 G. Hitoki, T. Takata, J. N. Kondo, M. Hara, H. Kobayashi and K. Domen, *Chem. Commun.*, 2002, 1698–1699.
168 M. Hara, G. Hitoki, T. Takata, J. N. Kondo, H. Kobayashi and K. Domen, *Catal. Today*, 2003, **78**, 555–560.
169 Z. Tong, S. Takagi, H. Tachibana, K. Takagi and H. Inoue, *J. Phys. Chem. B*, 2005, **109**, 21612–21617.
170 Z. W. Seh, J. Kibsgaard, C. F. Dickens, I. Chorkendorff, J. K. Nørskov and T. F. Jaramillo, *Science*, 2017, **355**, eaad4998.
171 X. Zong, J. Han, G. Ma, H. Yan, G. Wu and C. Li, *J. Phys. Chem. C*, 2011, **115**, 12202–12208.
172 Q. Wang, T. Hisatomi, Q. Jia, H. Tokudome, M. Zhong, C. Wang, Z. Pan, T. Takata, M. Nakabayashi, N. Shibata, Y. Li, I. D. Sharp, A. Kudo, T. Yamada and K. Domen, *Nat. Mater.*, 2016, **15**, 611–615.
173 B. Kraeutler and A. J. Bard, *J. Am. Chem. Soc.*, 1978, **100**, 4317–4318.
174 T. Takata, J. Jiang, Y. Sakata, M. Nakabayashi, N. Shibata, V. Nandal, K. Seki, T. Hisatomi and K. Domen, *Nature*, 2020, **581**, 411–414.
175 S. Das, A. Jangam, Y. Du, K. Hidajat and S. Kawi, *Chem. Commun.*, 2019, **55**, 6074–6077.
176 N. Sakamoto, H. Ohtsuka, T. Ikeda, K. Maeda, D. Lu, M. Kanehara, K. Teramura, T. Teranishi and K. Domen, *Nanoscale*, 2009, **1**, 106–109.
177 Y. Liu, H. Tsunoyama, T. Akita and T. Tsukuda, *J. Phys. Chem. C*, 2009, **113**, 13457–13461.
178 K. Maeda, K. Teramura, D. Lu, N. Saito, Y. Inoue and K. Domen, *Angew. Chem., Int. Ed.*, 2006, **45**, 7806–7809.
179 K. Maeda, K. Teramura, D. Lu, N. Saito, Y. Inoue and K. Domen, *J. Phys. Chem. C*, 2007, **111**, 7554–7560.
180 M. Yoshida, K. Takanabe, K. Maeda, A. Ishikawa, J. Kubota, Y. Sakata, Y. Ikezawa and K. Domen, *J. Phys. Chem. C*, 2009, **113**, 10151–10157.
181 K. Maeda, N. Sakamoto, T. Ikeda, H. Ohtsuka, A. Xiong, D. Lu, M. Kanehara, T. Teranishi and K. Domen, *Chem.–Eur. J.*, 2010, **16**, 7750–7759.
182 T. Ikeda, A. Xiong, T. Yoshinaga, K. Maeda, K. Domen and T. Teranishi, *J. Phys. Chem. C*, 2013, **117**, 2467–2473.
183 D. V. Goia and E. Matijević, *Colloids Surf., A*, 1999, **146**, 139–152.
184 K. Maeda, A. Xiong, T. Yoshinaga, T. Ikeda, N. Sakamoto, T. Hisatomi, M. Takashima, D. Lu, M. Kanehara, T. Setoyama, T. Teranishi and K. Domen, *Angew. Chem., Int. Ed.*, 2010, **49**, 4096–4099.
185 A. Xiong, T. Yoshinaga, T. Ikeda, M. Takashima, T. Hisatomi, K. Maeda, T. Setoyama, T. Teranishi and K. Domen, *Eur. J. Inorg. Chem.*, 2014, **2014**, 767–772.
186 T. Yoshinaga, M. Saruyama, A. Xiong, Y. Ham, Y. Kuang, R. Niishiro, S. Akiyama, M. Sakamoto, T. Hisatomi, K. Domen and T. Teranishi, *Nanoscale*, 2018, **10**, 10420–10427.
187 Y. Negishi, M. Mizuno, M. Hirayama, M. Omatoi, T. Takayama, A. Iwase and A. Kudo, *Nanoscale*, 2013, **5**, 7188–7192.
188 W. Kurashige, R. Kumazawa, Y. Mori and Y. Negishi, *J. Mater. Appl.*, 2018, **7**, 1–11.
189 Y. Negishi, Y. Matsuura, R. Tomizawa, W. Kurashige, Y. Niihori, T. Takayama, A. Iwase and A. Kudo, *J. Phys. Chem. C*, 2015, **119**, 11224–11232.
190 W. Kurashige, R. Kumazawa, D. Ishii, R. Hayashi, Y. Niihori, S. Hossain, L. V. Nair, T. Takayama, A. Iwase, S. Yamazoe, T. Tsukuda, A. Kudo and Y. Negishi, *J. Phys. Chem. C*, 2018, **122**, 13669–13681.
191 S. J. Tauster, S. C. Fung and R. L. Garten, *J. Am. Chem. Soc.*, 1978, **100**, 170–175.
192 S. J. Tauster, *Acc. Chem. Res.*, 1987, **20**, 389–394.
193 E. J. Braunschweig, A. D. Logan, A. K. Datye and D. J. Smith, *J. Catal.*, 1989, **118**, 227–237.
194 A. D. Logan, E. J. Braunschweig, A. K. Datye and D. J. Smith, *Langmuir*, 1988, **4**, 827–830.
195 A. A. Melvin, K. Illath, T. Das, T. Raja, S. Bhattacharyya and C. S. Gopinath, *Nanoscale*, 2015, **7**, 13477–13488.
196 S.-F. Hung, Y.-C. Yu, N.-T. Suen, G.-Q. Tzeng, C.-W. Tung, Y.-Y. Hsu, C.-S. Hsu, C.-K. Chang, T.-S. Chan, H.-S. Sheu, J.-F. Lee and H. M. Chen, *Chem. Commun.*, 2016, **52**, 1567–1570.
197 H. Bian, N. T. Nguyen, J. Yoo, S. Hejazi, S. Mohajernia, J. Müller, E. Spiecker, H. Tsuchiya, O. Tomanec, B. E. Sanabria-Arenas, R. Zboril, Y. Y. Li and P. Schmuki, *ACS Appl. Mater. Interfaces*, 2018, **10**, 18220–18226.
198 N.-T. Suen, S.-F. Hung, Q. Quan, N. Zhang, Y.-J. Xu and H. M. Chen, *Chem. Soc. Rev.*, 2017, **46**, 337–365.
199 Y. Zhang, N. Zhang, Z.-R. Tang and Y.-J. Xu, *J. Phys. Chem. C*, 2014, **118**, 5299–5308.
200 B. Han, S. Liu, N. Zhang, Y.-J. Xu and Z.-R. Tang, *Appl. Catal., B*, 2017, **202**, 298–304.
201 L. Yuan, C. Han, M.-Q. Yang and Y.-J. Xu, *Int. Rev. Phys. Chem.*, 2016, **35**, 1–36.
202 W. Kurashige, R. Hayashi, K. Wakamatsu, Y. Kataoka, S. Hossain, A. Iwase, A. Kudo, S. Yamazoe and Y. Negishi, *ACS Appl. Energy Mater.*, 2019, **2**, 4175–4187.
203 S. Trasatti, *J. Electroanal. Chem. Interfacial Electrochem.*, 1972, **39**, 163–184.
204 T. Hisatomi, K. Maeda, K. Takanabe, J. Kubota and K. Domen, *J. Phys. Chem. C*, 2009, **113**, 21458–21466.
205 K. Maeda, K. Teramura, H. Masuda, T. Takata, N. Saito, Y. Inoue and K. Domen, *J. Phys. Chem. B*, 2006, **110**, 13107–13112.
206 T. Ohno, L. Bai, T. Hisatomi, K. Maeda and K. Domen, *J. Am. Chem. Soc.*, 2012, **134**, 8254–8259.
207 K. Maeda, D. Lu, K. Teramura and K. Domen, *Energy Environ. Sci.*, 2010, **3**, 471–478.

208 W. Kurashige, Y. Mori, S. Ozaki, M. Kawachi, S. Hossain, T. Kawawaki, C. J. Shearer, A. Iwase, G. F. Metha, S. Yamazoe, A. Kudo and Y. Negishi, *Angew. Chem., Int. Ed.*, 2020, **59**, 7076–7082.
209 Y. Sakata, T. Hayashi, R. Yasunaga, N. Yanaga and H. Imamura, *Chem. Commun.*, 2015, **51**, 12935–12938.
210 T. H. Chiang, H. Lyu, T. Hisatomi, Y. Goto, T. Takata, M. Katayama, T. Minegishi and K. Domen, *ACS Catal.*, 2018, **8**, 2782–2788.
211 Y. Hang Li, J. Xing, Z. Jia Chen, Z. Li, F. Tian, L. Rong Zheng, H. Feng Wang, P. Hu, H. Jun Zhao and H. Gui Yang, *Nat. Commun.*, 2013, **4**, 2500.
212 D. Walsh, L. Arcelli, T. Ikoma, J. Tanaka and S. Mann, *Nat. Mater.*, 2003, **2**, 386–390.
213 T. Oshima, D. Lu, O. Ishitani and K. Maeda, *Angew. Chem., Int. Ed.*, 2015, **54**, 2698–2702.
214 E. Cui and G. Lu, *J. Phys. Chem. C*, 2013, **117**, 26415–26425.
215 E. Cui and G. Lu, *Int. J. Hydrogen Energy*, 2014, **39**, 7672–7685.
216 Y. Zhang, D. A. J. M. Ligthart, X.-Y. Quek, L. Gao and E. J. M. Hensen, *Int. J. Hydrogen Energy*, 2014, **39**, 11537–11546.
217 M. Hojamberdiev, M. M. Khan, Z. Kadirova, K. Kawashima, K. Yubuta, K. Teshima, R. Riedel and M. Hasegawa, *Renewable Energy*, 2019, **138**, 434–444.
218 M. Luo, P. Lu, W. Yao, C. Huang, Q. Xu, Q. Wu, Y. Kuwahara and H. Yamashita, *ACS Appl. Mater. Interfaces*, 2016, **8**, 20667–20674.
219 S. Xu, A. J. Du, J. Liu, J. Ng and D. D. Sun, *Int. J. Hydrogen Energy*, 2011, **36**, 6560–6568.
220 Q. Wu, S. Xiong, P. Shen, S. Zhao, Y. Li, D. Su and A. Orlov, *Catal. Sci. Technol.*, 2015, **5**, 2059–2064.
221 X. L. Du, X. L. Wang, Y. H. Li, Y. L. Wang, J. J. Zhao, L. J. Fang, L. R. Zheng, H. Tong and H. G. Yang, *Chem. Commun.*, 2017, **53**, 9402–9405.
222 C. P. Joshi, M. S. Bootharaju, M. J. Alhilaly and O. M. Bakr, *J. Am. Chem. Soc.*, 2015, **137**, 11578–11581.
223 X. Kang, S. Chen, S. Jin, Y. Song, Y. Xu, H. Yu, H. Sheng and M. Zhu, *ChemElectroChem*, 2016, **3**, 1261–1265.
224 C. Wang, P. Lv, D. Xue, Y. Cai, X. Yan, L. Xu, J. Fang and Y. Yang, *ACS Sustainable Chem. Eng.*, 2018, **6**, 8447–8457.
225 L. Tian, Y. Luo, K. Chu, D. Wu, J. Shi and Z. Liang, *Chem. Commun.*, 2019, **55**, 12976–12979.
226 H. Hata, Y. Kobayashi, V. Bojan, W. J. Youngblood and T. E. Mallouk, *Nano Lett.*, 2008, **8**, 794–799.
227 J. Zhang, M. Grzelczak, Y. Hou, K. Maeda, K. Domen, X. Fu, M. Antonietti and X. Wang, *Chem. Sci.*, 2012, **3**, 443–446.
228 H. Suzuki, S. Nitta, O. Tomita, M. Higashi and R. Abe, *ACS Catal.*, 2017, **7**, 4336–4343.
229 A. Miyoshi, J. J. M. Vequizo, S. Nishioka, Y. Kato, M. Yamamoto, S. Yamashita, T. Yokoi, A. Iwase, S. Nozawa, A. Yamakata, T. Yoshida, K. Kimoto, A. Kudo and K. Maeda, *Sustainable Energy Fuels*, 2018, **2**, 2025–2035.
230 D. Bahnemann, A. Henglein, J. Lilie and L. Spanhel, *J. Phys. Chem.*, 1984, **88**, 709–711.
231 H. N. Ghosh, J. B. Asbury and T. Lian, *J. Phys. Chem. B*, 1998, **102**, 6482–6486.
232 B. Ohtani, R. M. Bowman, D. P. Colombo, Jr., H. Kominami, H. Noguchi and K. Uosaki, *Chem. Lett.*, 1998, **27**, 579–580.
233 A. Yamakata, T.-a. Ishibashi and H. Onishi, *Chem. Phys. Lett.*, 2001, **333**, 271–277.
234 T. Yoshihara, R. Katoh, A. Furube, Y. Tamaki, M. Murai, K. Hara, S. Murata, H. Arakawa and M. Tachiya, *J. Phys. Chem. B*, 2004, **108**, 3817–3823.
235 J. Lee, H. S. Shim, M. Lee, J. K. Song and D. Lee, *J. Phys. Chem. Lett.*, 2011, **2**, 2840–2845.
236 X.-Q. Gong, A. Selloni, O. Dulub, P. Jacobson and U. Diebold, *J. Am. Chem. Soc.*, 2008, **130**, 370–381.
237 M. R. Nellist, F. A. L. Laskowski, J. Qiu, H. Hajibabaei, K. Sivula, T. W. Hamann and S. W. Boettcher, *Nat. Energy*, 2018, **3**, 46–52.
238 M. R. Nellist, J. Qiu, F. A. L. Laskowski, F. M. Toma and S. W. Boettcher, *ACS Energy Lett.*, 2018, **3**, 2286–2291.
239 G. N. Vayssilov, Y. Lykhach, A. Migani, T. Staudt, G. P. Petrova, N. Tsud, T. Skála, A. Bruix, F. Illas, K. C. Prince, V. Matolín, K. M. Neyman and J. Libuda, *Nat. Mater.*, 2011, **10**, 310–315.
240 K. He, J. Xie, Z.-Q. Liu, N. Li, X. Chen, J. Hu and X. Li, *J. Mater. Chem. A*, 2018, **6**, 13110–13122.
241 J. Schneider, M. Matsuoka, M. Takeuchi, J. Zhang, Y. Horiuchi, M. Anpo and D. W. Bahnemann, *Chem. Rev.*, 2014, **114**, 9919–9986.
242 S. Zhao, R. Jin, H. Abroshan, C. Zeng, H. Zhang, S. D. House, E. Gottlieb, H. J. Kim, J. C. Yang and R. Jin, *J. Am. Chem. Soc.*, 2017, **139**, 1077–1080.
243 W. Zhu, Y.-J. Zhang, H. Zhang, H. Lv, Q. Li, R. Michalsky, A. A. Peterson and S. Sun, *J. Am. Chem. Soc.*, 2014, **136**, 16132–16135.
244 B. Kumar, T. Kawawaki, N. Shimizu, Y. Imai, D. Suzuki, S. Hossain, L. V. Nair and Y. Negishi, *Nanoscale*, 2020, **12**, 9969–9979.
245 Y. Negishi, T. Kawawaki, Y. Imai, D. Suzuki, S. Kato, I. Kobayashi, T. Suzuki, R. Kaneko and S. Hossain, *Chem.–Eur. J.*, 2020, DOI: 10.1002/chem.202001877.
246 R. Li, F. Zhang, D. Wang, J. Yang, M. Li, J. Zhu, X. Zhou, H. Han and C. Li, *Nat. Commun.*, 2013, **4**, 1432.
247 Y. Negishi, S. Hashimoto, A. Ebina, K. Hamada, S. Hossain and T. Kawawaki, *Nanoscale*, 2020, **12**, 8017–8039.